Research Progress on Organic-Inorganic Halide Perovskite Materials and Solar Cells

Luis K. Ono[†], *Yabing Qi*[†,*]

[†] Energy Materials and Surface Sciences Unit (EMSS), Okinawa Institute of Science and Technology Graduate University (OIST), 1919-1 Tancha, Onna-son, Okinawa 904-0495 Japan.

*Corresponding author. E-mail: Yabing.Qi@OIST.jp

Keywords: Perovskite solar cell, efficiency, stability, upscaling

Abstract:

Owing to the intensive research efforts across the world since 2009, perovskite solar cell power conversion efficiencies (PCEs) are now comparable or even better than several other photovoltaic (PV) technologies. In this topical review article, we review recent progress in the field of organic-inorganic halide perovskite materials and solar cells. We associate these achievements with the fundamental knowledge gained in the perovskite research. The major recent advances in the fundamental perovskite material and solar cell research are highlighted, including the current efforts in visualizing the dynamical processes (*in operando*) taking place within a perovskite solar cell under operating conditions. We also discuss the existing technological challenges. Based on a survey of recently published works, we point out that to move the perovskite PV technology forward towards the next step of commercialization, what perovskite PV technology need the most in the coming next few years is not only further PCE enhancements, but also up-scaling, stability, and lead-toxicity.

1. Introduction

Photovoltaic technology (PV) is often aforementioned as a solution to issues related to increase in global electricity demands and global warming [1]. Globally installed PV capacity reached 237 GWp at the end of 2015. This number is equivalent to only ~1% of worldwide electricity demands [1, 2]. A myriad of PV materials and technologies were developed in the

last few decades with the aim to fabricate solar cells with low cost, high solar-to-energy power conversion efficiency, long-term lifetime, and environmental friendliness [3-5]. Flexibility and light-weight are also important for specific application needs (e.g., flexible electronics, building-integrated PV systems, etc.). Among the various types of PV technologies, organic-inorganic halide perovskite (PVSK) based solar cells have emerged as a competitive candidate for the next generation high solar-to-electricity efficiency PV technology that is compatible with low-cost, low-temperature processing, flexible substrates, and large-area fabrication using, e.g., ultrasonic spray-coating, printing, roll-to-roll, and vapor deposition techniques [6-9]. Laboratory scale cells (active area < 0.3 cm^2) with the certified highest PCE of 22.7% have been achieved with a relatively short period of time since solid-state hole transport layer (HTL) was implemented [10-15]. These achievements are important grand merits when compared to Si or GaAs PV technologies, which require cost- and energy-demanding facilities for fabrication processes. In this topical review, we share our views regarding *what does perovskite PV technology need the most in the coming next few years*. To move PVSK-based solar cell technology forward towards commercialization, there are several crucial issues that need to be addressed: (i) up-scalable and reproducible process (controllable thin-film growth and deposition) with compatibility with low-cost and high-throughput, (ii) high stability and long lifetime testing data, and (iii) low toxicity. This topical review introduces the most recent advances in PVSK solar cells and modules that are essential for the next step commercialization. At the end of this review we outline the new trends and future directions in PVSK solar cell research.

2. Power conversion efficiencies in perovskite-based solar cells

On the basis of published works worldwide and recent trends compared to other PV technologies [10, 11], there is no doubt that exceptional PCEs can be achieved in PVSK solar cells (figure 1). Furthermore, because the optimal band gap (E_g) for a single-junction solar cell is between 1.1 eV and 1.4 eV according to the Shockley-Queisser (S-Q) model [16, 17], further strategies are expected to give rise to even higher efficiencies [18]. Theoretical calculations (S-Q limit) predict that the limiting PCE for single-junction solar cell is 33.7% for an optimum semiconductor with E_g = 1.34 eV. Recently, Polman et al. [19] analyzed the electrical characteristics of record-efficiency cells made from 16 widely studied PV materials (figure 1a). PVSK solar cells have already achieved at least ~70% of this limit for E_g of 1.6 eV (figure 1b). As comparison, GaAs PVs (E_g = 1.35 eV, PCE = 28.8%) have achieved ~85% of the predicted

limit. A new world record efficiency of 22.7% in PVSK solar cells [10, 11] was achieved only recently since March 2016. Naturally, a question arises: what strategies need to be further considered in PVSK fundamental research and technological aspects to overcome further this barrier of 22.7%? Because the efficiency of any PV systems is a key driver to reduce the cost of electricity generation, achievement of higher efficiency in PVSK-based solar cells and modules is highly desirable. In Si solar cell research, after 18 years have passed without a significant increase in PCE, the Kaneka R&D group this year announced a new record PCE of 26.3% monocrystalline Si over >180 cm^2 area [20, 21].

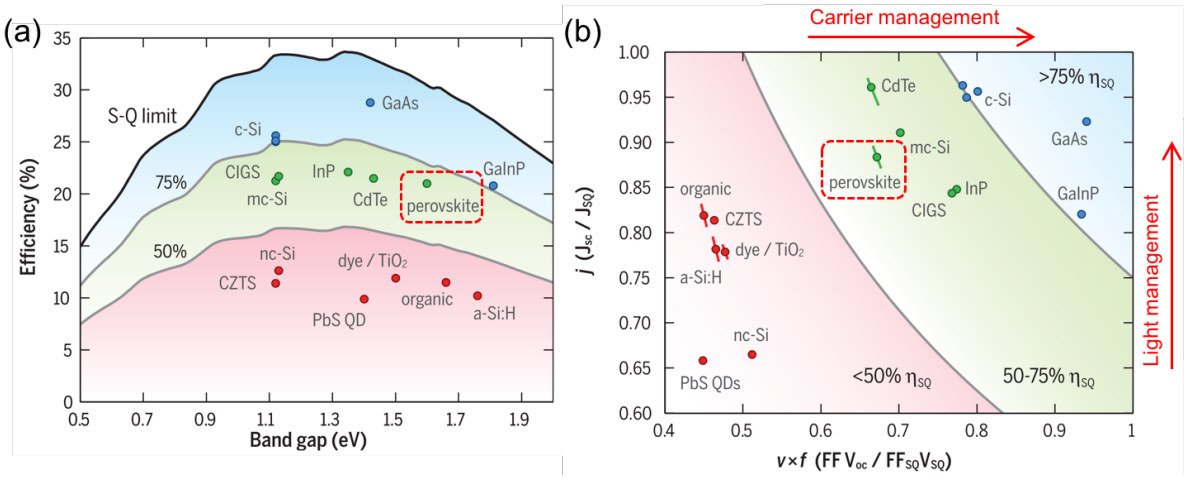

Figure 1. (a) World record-efficiencies of different PV technologies compared to the theoretical Shockley-Queisser detailed-balance limit as a function of band gap. (b) The ratio (J_{sc} / J_{SQ}) versus (V_{oc} × FF / V_{SQ} × FF_{SQ}) plot for record-efficiency cells. Light management and carrier management arrows are indicative of what a particular PV material need to improve for attaining higher efficiencies. Colors correspond to cells achieving <50% of their S-Q efficiency limit (red region), 50% to 75% (green region), and >75% (blue region). The record efficiency shown for PVSK solar cell in this figure corresponds to the 20.1% cell employing mixed cation-anion $(FAPbI_3)_{0.95}(MA_{0.15}PbBr_3)_{0.05}$ [22]. Reprinted with permission from Ref. [19]. Copyright 2016 American Association for the Advancement of Science (AAAS).

On the basis of published studies, issues in devices showing lower short-circuit current density (J_{sc}) than the S-Q limit is associated with (i) incomplete light absorption and/or (ii) incomplete transport and collection of generated carriers. Another cause for J_{sc} loss in solar cells is related to parasitic absorption in adjacent layers to the absorber and the back reflectors [17]. Complementary to above observations, the reduced open-circuit voltage (V_{oc}) or fill factor (FF) are associated with (iii) bulk, surfaces, and/or interfacial carrier recombination, parasitic series and/or shunting resistance, or other electrical non-idealities [19, 23-26]. figure

1b shows a comprehensive comparison of several widely studied PV technologies regarding their optical (light management) and electronic (carrier management) [19]. The light management parameter ($j = J_{sc} / J_{SQ}$) and carrier management ($v \times f = V_{oc} \times FF / V_{SQ} \times FF_{SQ}$) were used as figures of merit to compare their electrical characteristics and evaluate to what degree the cell efficiency is limited by light management or carrier management [19]. A notable merit of solution-processed PVSK solar cells is the relatively small voltage loss (V_{oc} / V_{SQ}) that is even better than record-efficiency monocrystalline Si homojunction cells. However, the photocurrent loss (J_{sc} / J_{SQ}) and decreased fill factor (FF / FF_{SQ}) in PVSK solar cells are still substantial [19].

Considering a particular case of $MAPbI_3$ PVSK that corresponds to a most widely studied PVSK material system in literature, the absorption coefficient is among the highest of all photovoltaic materials (>3×10^4 cm^{-1}, figure 2a) and is more than one order of magnitude greater than that of Si (figure 2a). This enhanced light absorption characteristics in PVSKs was associated with the inherent formation of a direct-band gap and enhanced light coupling in Pb 6*p*–I 5*p* transitions in $MAPbI_3$ PVSK [18, 27, 28]. Crystalline Si (c-Si) shows a much lower absorption coefficient because of its indirect band gap and shows signatures related to phonon-assisted absorption (inset in figure 2a). In many cases, photocurrent loss issues are closely associated with film quality (imperfections and defects) [29, 30]. The UV-Visible (UV-Vis) absorption spectrum of PVSKs was shown to generate a sharp absorption edge, comparable to those of CdTe and GaAs, which are considered as the best semiconductor absorbers (figure 2a). Based on this absorption edge position and slope, we can determine not only the optical band gap, but also the information regarding material microstructure (imperfections and defects) by analyzing the exponential decay of the sub-band gap absorbance, commonly described by the empirical Urbach rule. The equation of the empirical Urbach rule is $A \propto \exp(E/E_0)$, where A is absorbance, E photon energy, and E_0 the characteristic Urbach energy representing the width of the exponential Urbach tail (figure 2a) [23, 31-33]. Despite the fact that there is no theoretical derivation for the Urbach rule, a general consensus exists that the Urbach tail in crystalline semiconductors is related to the static (structural disorder) and/or dynamic (phonon) disorder, that arises from lattice point defects, dislocations, strain, deviation from ideal stoichiometry, and grains [23, 31-33]. Pure $MAPbI_3$ and $MAPbBr_3$ ($MA = CH_3NH_3$) perovskites have sharp absorption edges with low Urbach energy of ~15-27 meV and ~23-34 meV, respectively [23, 31-33]. Compared to other semiconductors (figure 2a), the Urbach

energy of $MAPbI_3$ is close to that of GaAs (a monocrystalline direct band gap semiconductor and typically obtained using an expensive production process). This example highlights one of the major advantage of PVSK solar technology, i.e., PVSKs can retain a high quality even when prepared using low-cost processes (e.g., solution processes).

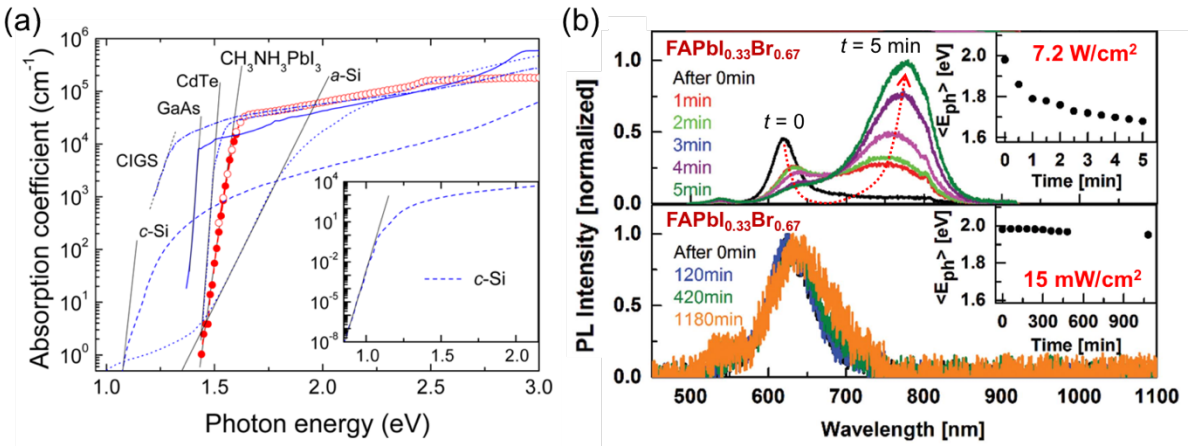

Figure 2. (a) Absorption coefficient of $CH_3NH_3PbI_3$ compared to other PV materials of amorphous-Si (a-Si), GaAs, $Cu(In,Ga)Se_2$ (CIGS), CdTe, and crystalline Si (c-Si) corresponding to room temperature measurements. Slope of Urbach tail is shown for each material. The inset shows the data for c-Si down to low absorption values. (b) PL spectra of $FAPb(Br_{0.67}I_{0.33})_3$ film over 5 min of continuous illumination following excitation at 400 nm with intensity of 7.2 W/cm^2 and 15 mW/cm^2. Inset: Change of the average photon energy $<E_{ph}>$ as a function of time. (a) Reprinted with permission from ref. [31]. Copyright 2014 American Chemical Society. (b) Reprinted with permission from ref. [34]. Copyright 2015 WILEY-VCH Verlag GmbH & Co. KGaA, Weinheim.

3. Dynamical processes in perovskite solar cells influencing power conversion efficiencies.

Often a transient behavior in solar cell parameters (Jsc, Voc, FF, and PCE) are observed during the initial measurements (e.g., light-soaking). As described later, the PVSK solar cell structure is complex and multiple dynamical processes result in the overall PCE variations as a function of time. Deconvolution of these dynamical processes are important to further develop strategies of stable PVSK solar cells. As an example, a dynamical process taking place in mixed $MAPbI_{3-x}Br_x$, PVSKs was first reported by Hoke et al. [35]. The initially homogeneous $MAPb(Br_xI_{1-x})_3$ ($0.2 < x < 0.9$) PVSK films were observed to undergo photoexcited phase-separation into two phases, one iodine-rich and the other bromide-rich

domain in the same film, confirmed by photoluminescence (PL) peak splitting and corroborated by X-ray diffraction (XRD). Interestingly, when allowed to relax in dark, the PL pattern returned to its original single phase state, meaning that the dynamical process is reversible. Changing the cation from MA to FA ($FAPbI_{3-x}Br_x$), a similar behavior was also reported (figure 2b) [34]. The intensity of the excitation laser is an important parameter in producing phase segregation (figure 2b). The PL emission of $FAPb(Br_{0.67}I_{0.33})_3$ films recorded for laser excitation with an intensity of 7.2 W/cm^2 following 5 min of continuous illumination showed the gradual decrease and shift of the 620 nm (~2 eV) to a new dominant low-energy PL feature at ~785 nm (1.58 eV). On the other hand, when an identical $FAPb(Br_{0.67}I_{0.33})_3$ film was illuminated at the same wavelength (400 nm) with a lower laser intensity of 15 mW/cm^2, no changes in PL spectra were observed even after 1180 min (~20 h) (figure 2b). Compared to the $MAPbI_{3-x}Br_x$ system, it was reported that light intensity as low as 1.2 mW/cm^2 with continuous illumination (10 min) can induce phase segregation [36]. Because photovoltaic devices are typically tested under AM1.5 conditions (100 mW/cm^2), it is necessary to develop strategies to make PVSK systems resilient to phase segregation. A number of reports proposed the microscopic origins for the phase-segregation phenomena [35-43] and was recently summarized in ref. [18]. Naturally occurring small variations in perovskite composition after sample preparation were proposed as origin for phase-segregation phenomena inducing iodide-rich domains with a reduced band gap. Therefore, compositional homogeneity in PVSK materials and crystallinity are the determining factors for stability [37, 40, 42-50]. The broadening of the PL peak quantified by the full-width at half maximum (fwhm) is also an important indicator of the presence of trap densities and morphological disorder and thus correlating with Urbach energy [32, 33]. The fundamental reversible mechanisms driving halide-segregation (upon light) and remixing (in dark) are yet to be developed [18, 30, 41, 42, 51].

Based on several reports, efforts are being made to study the PVSK dynamics under more realistic solar cell operation conditions. For instance, the micro-PL technique was demonstrated to be successful in mapping spatially resolved phase segregation in an active layer of a complete solar cell device [52]. Duong et al. reported that $Rb_{0.05}(Cs_{0.1}FA_{0.75}MA_{0.15})_{0.95}PbI_2Br$ suffers from light-induced phase segregation within the active area when the cell is operated under open-circuit conditions (figure 3). However, phase-segregation within the active area is negligible when the cells are operated under maximum power point (MPP) or J_{sc} [52]. This highlights the importance of studies in establishing the connection between the dynamical processes in solar cell devices and operation conditions.

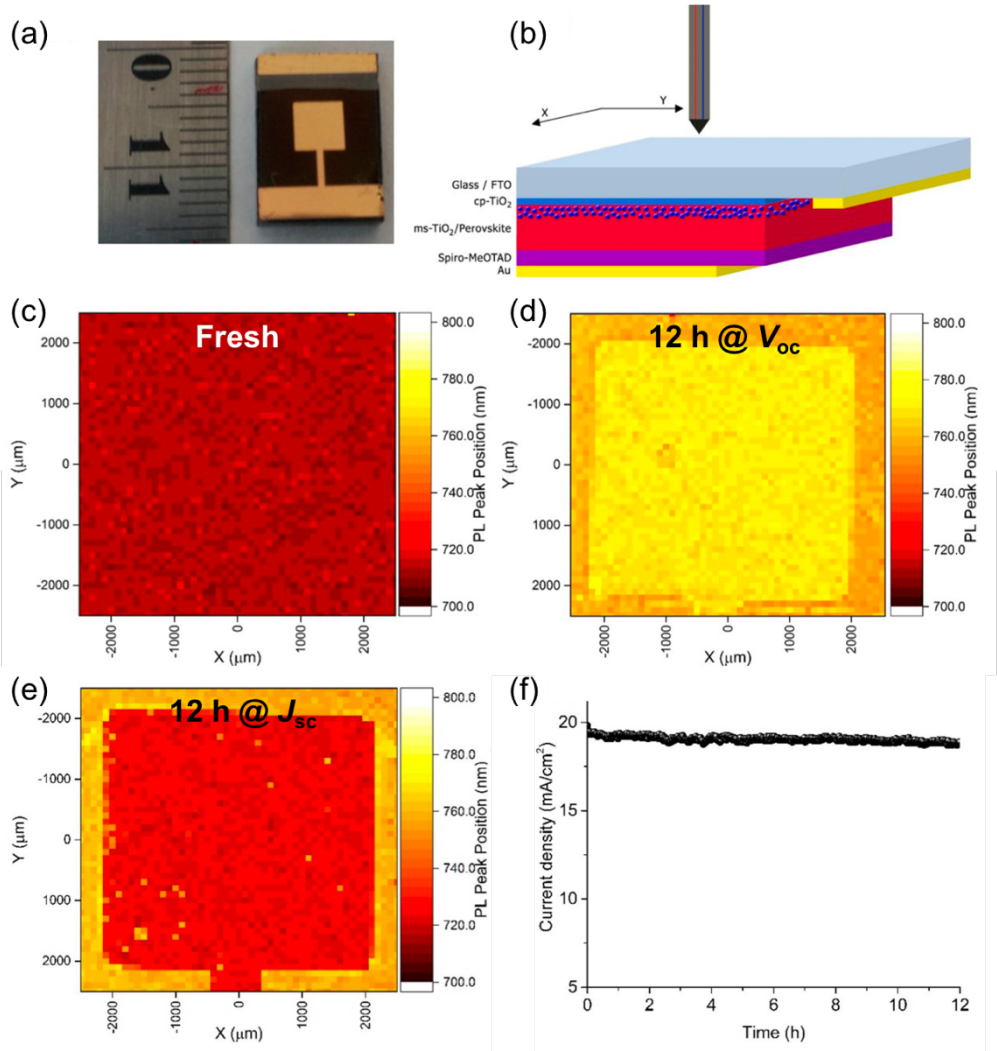

Figure 3. (a) Non-encapsulated $Rb_{0.05}(Cs_{0.1}FA_{0.75}MA_{0.15})_{0.95}PbI_2Br$ based PVSK solar cell with an active area of ~0.18 cm^2 and (b) micro-PL scanning measurement setup performed in air at RT. 2D mapping shows PL peak position distribution scanned over an area of 5 × 5 mm^2 on (c) fresh device and after 12 h under one sun illumination at (d) V_{oc} and (e) J_{sc}. (f) Jsc monitoring corroborates enhanced stability. Reprinted with permission from ref. [52]. Copyright 2017 American Chemical Society.

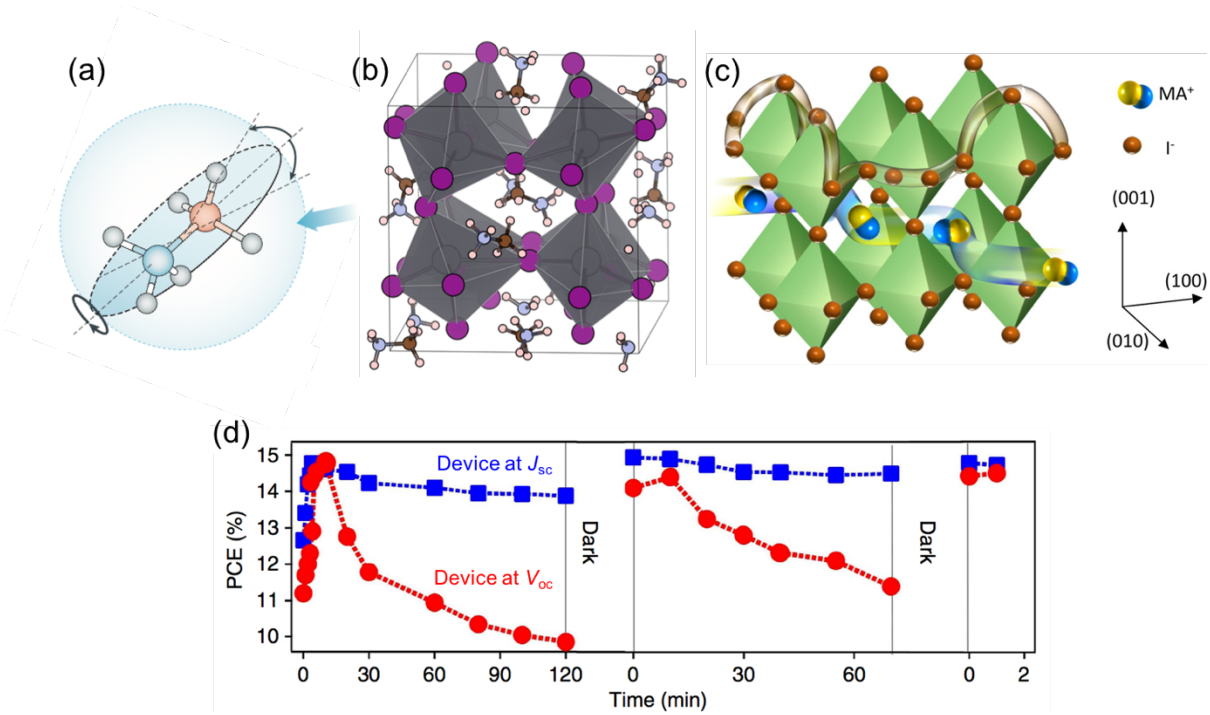

Figure 4. (a) Dynamic orientational disorder of MA molecules (b) disturbs the metal-halide lattice inducing distortion. (c) Illustration of proposed migration path of I^- ions along the I^--I^- edge of the PbI_6 octahedra in $MAPbI_3$. MA^+ migration was also corroborated experimentally. (d) Time evolution of device performance under one sun illumination and after resting in dark. Devices were stresses at Jsc (blue squares) or at Voc (red circles). (a) Reprinted with permission from ref. [25]. Copyright 2017 MacMillan Publishers Limited. (b) Reprinted with permission from ref. [53]. Copyright 2015 American Chemical Society. (c) Reprinted with permission from ref. [54]. Copyright 2016 American Chemical Society. (d) Reprinted with permission from ref. [55]. Copyright 2016 MacMillan Publishers Limited.

PVSK materials can be considered to possess a "soft" (or "plastic") crystalline structure [56, 57] formed by ions exhibiting rich dynamical processes such as (i) organic cation rotations (figure 4a) [58-67], (ii) inorganic lattice deformation (figure 4b) [61, 68], and (iii) ion migration [25, 54] (figure 4c). The dynamics of organic cations determine the structural, electronic, and optical properties of PVSKs because the cation dynamics disturbs the metal-halide (e.g., Pb–I–Pb) lattice. As consequence, the deformation of metal-halide lattice is associated with several local effects such as (i) dynamic direct-to-indirect transitions in bandgap suppressing charge recombination [62, 69]; (ii) nanoscale ferroelectric domains (due to the MA^+ cation dipole moment) can assist separation of electrons and holes reducing their recombination [70, 71]; (iii) spatially separated localization of valence and conduction bands [66]; (iv) Rashba

effect [57, 72], (v) large polaron formation [66, 73], and (vi) conductivity along charged domains is enhanced due to charge accumulation [74]. The above mentioned fundamental dynamical processes contribute to the superior solar conversion efficiency in PVSKs. It has been reported that absorption coefficients and charge transport properties of surfaces differ significantly from their bulk properties, such as morphology, carrier mobility, photocurrent, carrier dynamics, optical band gap, and device performance [25, 75-79]. For instance, ions in PVSKs migrate (figure 4c) under the influence of an electric field during device operation [25, 54]. Such migration occurs mainly through defects in the lattice. Based on time-resolved photoluminescence techniques, a larger surface-trap density of $\sim 1.6\times10^{17}$ cm^{-3} was reported compared to bulk trap densities of $\sim 5\times10^{16}$ cm^{-3} [24]. Therefore, interface properties have dominant effects in many cases. For example, under light and applied bias conditions, accumulation of ions and vacancies at interfaces formed between adjacent layers (ETL/PVSK/HTL) creates further additional electronic trap states at interfaces leading to a partial screening of the built-in potential. As consequence, charge extraction efficiency deteriorates leading to lower device performance as operation time evolves (figure 4d) [55, 80, 81]. When these PVSK solar cells operate under controlled mild conditions, their performance recovers (self-healing) to the original value after resting in dark [55, 82]. As exemplified above, understanding of fundamental dynamical processes taking place at the buried interfaces in PVSK solar cell devices are imperative for the design of next generation PVSK solar cells.

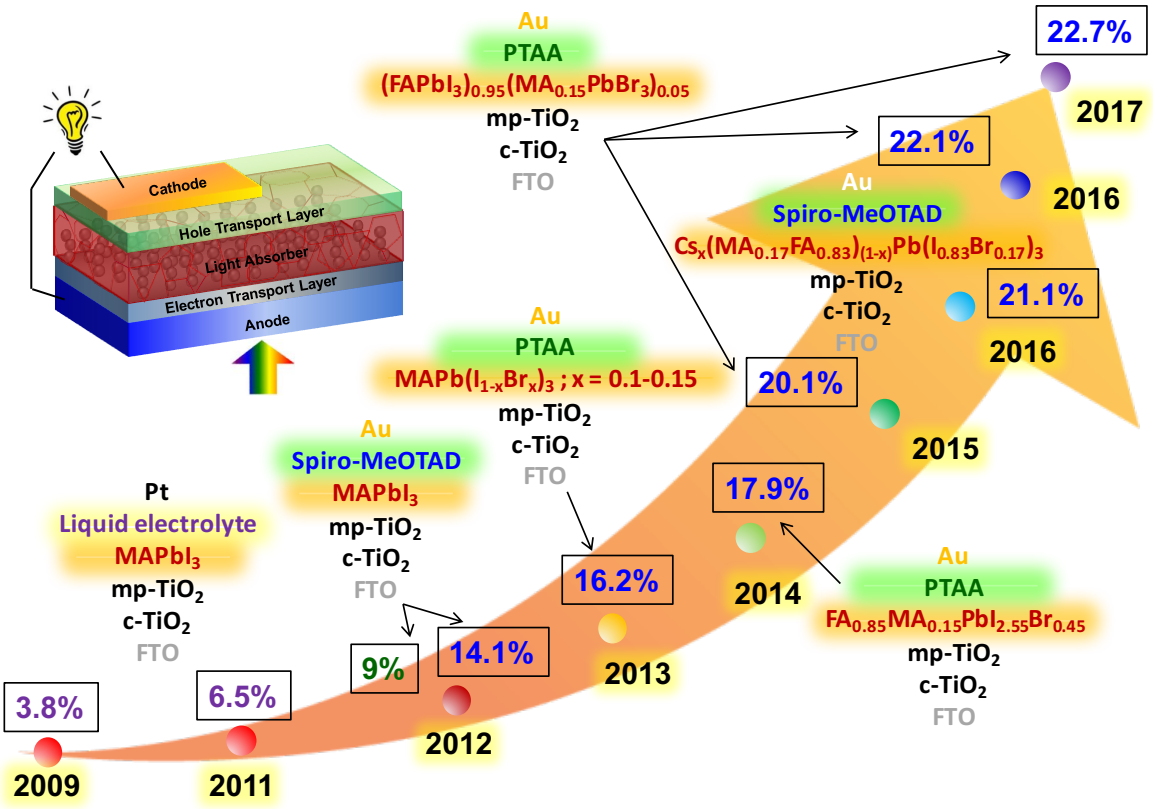

Figure 5. Selected lab-scale PVSK solar cell efficiencies evolved over the years. The certified efficiencies by NREL a represented by blue-colored numbers [10, 11].

As listed in figure 5, notably, the best-performing lab-scale PVSK solar cells share the same device (regular) structure comprising of FTO (anode)/c-TiO_2+mp-TiO_2 (ETL)/PVSK (absorber)/organic based HTL/Au (cathode); where FTO = fluorine-doped tin oxide, c = compact, and mp = mesoporous. Alternative structures such as planar structure, inverted structure [83] (PCE ~ 20%), HTL-free [84, 85], carbon counter electrode [86, 87] based solar cells have been proposed, but their PCEs are somewhat behind compared to that of the regular structure. In these device structures, different functional layers are stacked on top of each other producing multiple interfaces. What physico-chemical properties (i.e., morphology, interface atomic structure, and stoichiometry) influence charge transfer processes across interfaces are of important questions; these impact the overall device performance. Inclusion of selective contacts (ETL and HTL) was often a common practice to ensure efficient charge extraction from the perovskite layer. With the application of ETL and HTL, charge recombination processes were still shown to majorly take place at the interfaces due to generally higher density of interfacial defects compared to PVSK bulk counterpart [24, 88-90]. Furthermore, asymmetry in diffusion lengths for electrons and holes in PVSK solar cells caused by (i) unbalanced charge

extraction, (ii) potential barriers, and (iii) interfacial trap states were reported to prevent the device from reaching high PCEs [91-93]. To understand the mechanism of charge transport and to optimize device structure, it is necessary to determine the complete band diagram formed not within the bulk of individual functional material, but also at the interfaces (interfacial energetics) in these PVSK solar cells. Kelvin probe force microscopy (KPFM) was shown to be a versatile technique providing the potential landscape distribution across the multiple interfaces formed by the stacked layers constituting the solar cell device [92-97]. Alternatively, despite the fact that PES is a surface sensitive technique, strategies to probe the buried interface was reported by performing *in situ* incremental material deposition [98-115]. These works provide a more realistic picture of energy levels at interfaces such as band bending and interfacial dipoles than the assumption of a simple flat-band alignment between two adjacent materials (figure 6a) [77, 79, 98, 99, 105, 116-119]. Furthermore, PES was further employed to determine the corresponding energy positions of trap states in PVSKs (figure 6b) [120, 121] as well as valence band dispersion employing angle resolved PES (ARPES, figure 6c) [122, 123]. Knowing the band structures as well as density of trap states [124, 125] in PVSKs and their corresponding energy positions are important for the overall understanding of electronic properties and charge transport characteristics.

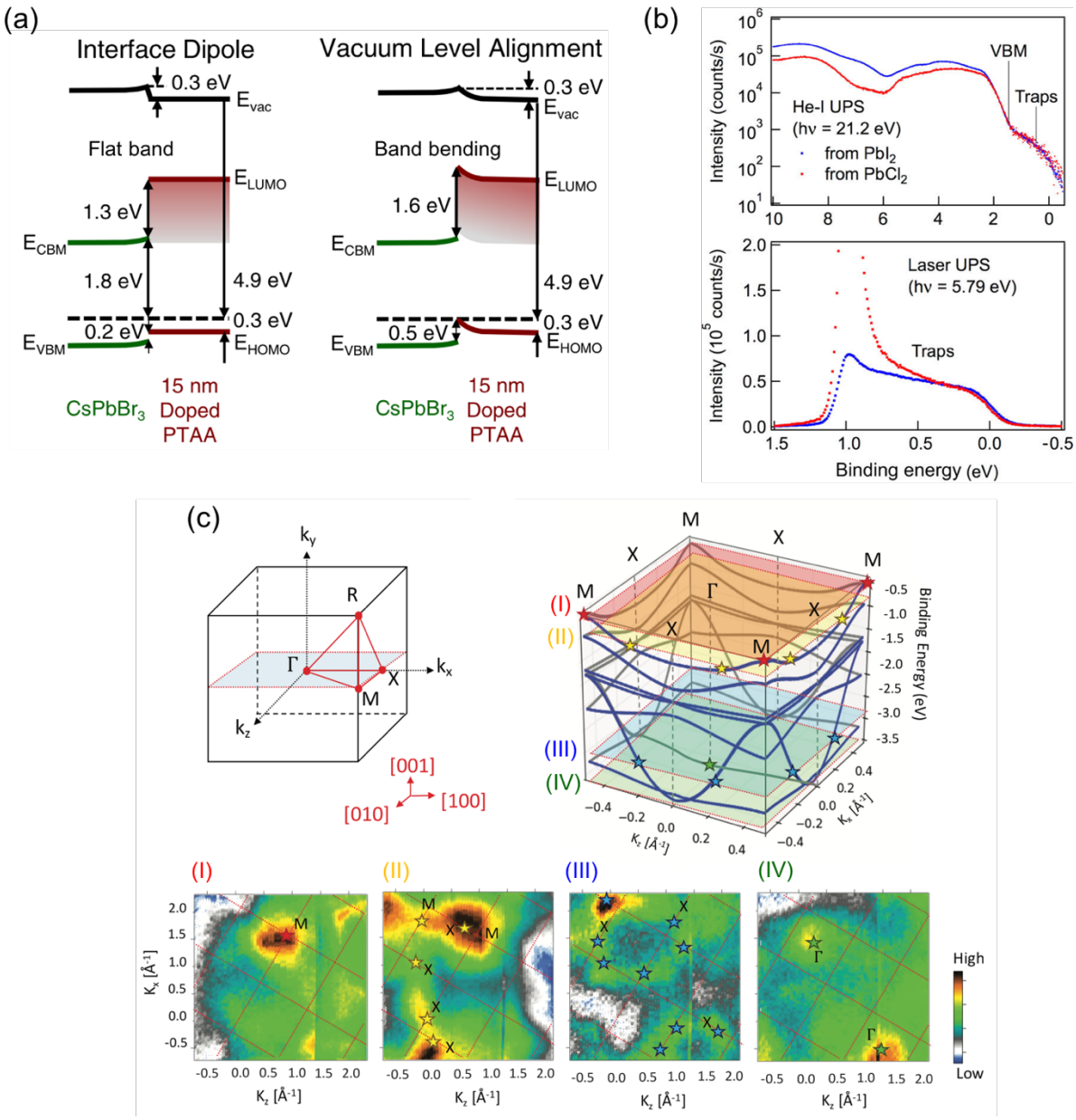

Figure 6. (a) Schematic energy level diagrams of the interface between $CsPbBr_3$ PVSK and PTAA HTL determined by UPS measurements. (b) Trap states determined by UPS with hν = 21.22 eV (top) and 5.79 eV (bottom) on PVSK film prepared on Si with native oxide by vapor deposition of MAI and PbI_2 (blue) or $PbCl_2$ (red) precursors. (c) angle-resolved photoemission spectroscopy probed on cleaved $MAPbI_3$ single crystal. (a) Reprinted with permission from ref. [105]. Copyright 2017 American Institute of Physics Publishing. (b) Reprinted with permission from ref. [122]. Copyright 2017 American Chemical Society.

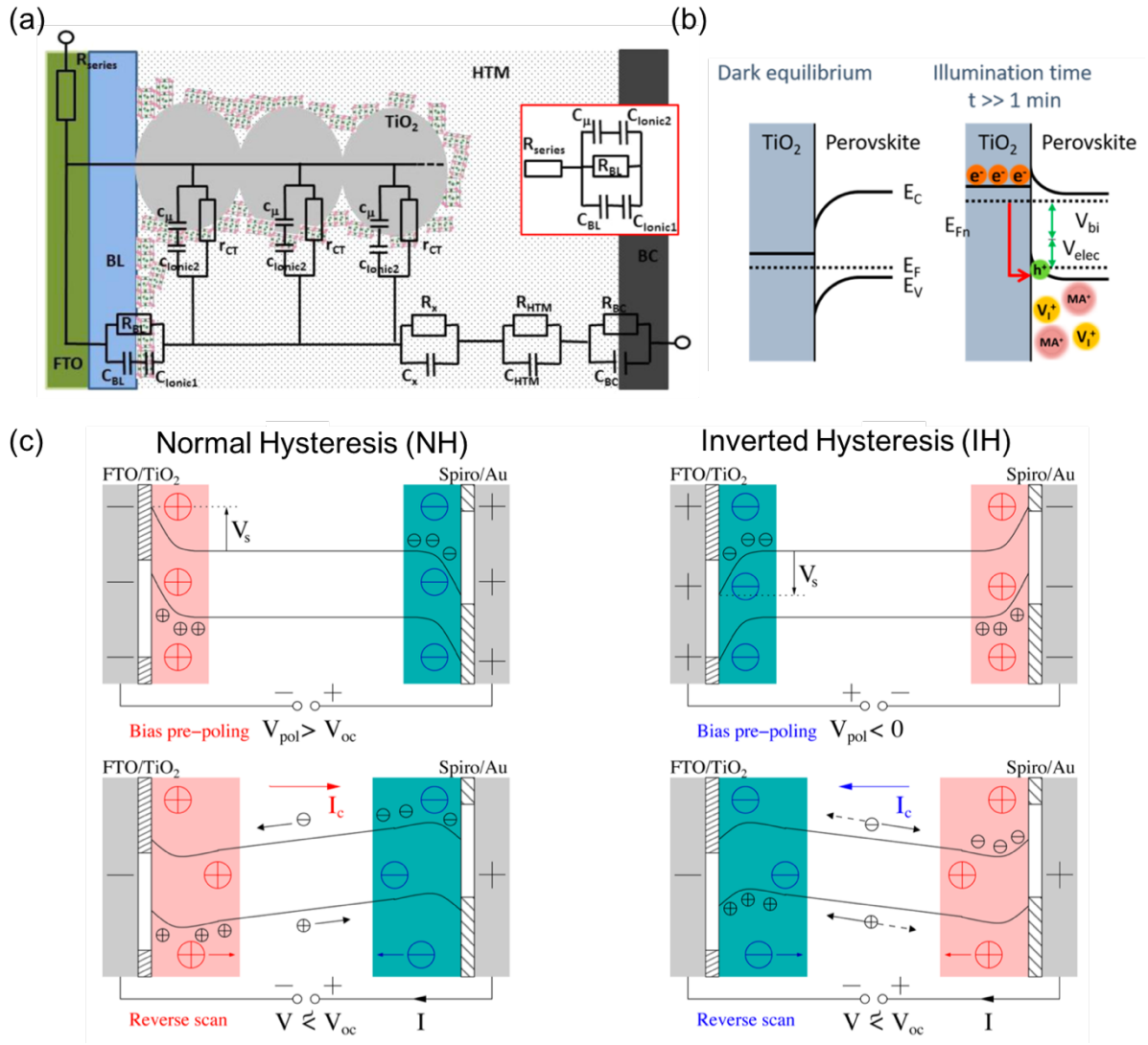

Figure 7. (a) Proposed equivalent circuit for PVSK solar cell. Further detailed discussion of this figure is provided in ref. [126]. (b) Energy diagram at TiO_2/PVSK contact in V_{oc} condition at two different stages: (a) under dark where ion migration is suppressed and (b) after a substantial migration event of cations and vacancies took place induced by light (t >> 1 min). Red arrow represents major interfacial charge recombination. V_{elec} is the electrostatic potential that contributes to the built-in potential (V_{bi}). (c) Schematic of band diagram of bias pre-poled devices. The bias pre-poling condition (Vpol) determines the NH ($V_{pol} > V_{oc}$) or IH ($V_{pol} < 0$) conditions. Further detailed discussion of this figure is provided in ref. [127]. (a) Reprinted with permission from ref. [126]. Copyright 2014 American Chemical Society. (b) Reprinted with permission from ref. [128]. Copyright 2017 American Chemical Society. (c) Reprinted with permission from ref. [127]. Copyright 2017 American Chemical Society.

The simultaneous access to the multiple buried interfaces in PVSK solar cells is a grand challenge. This situation is made even more complex when considering the additional necessity to "watch" dynamical processes occurring in PVSK solar cells under operation conditions. Impedance spectroscopy (IS) was demonstrated as a powerful tool for studying buried interfaces providing comprehensive equivalent circuits (figure 7a) [126, 129-133]. Furthermore, it is able to probe the dynamics of ions and charge carriers transport under solar cell operation conditions (figure 7b) [128, 134-136]. The working principle is based on capturing the modulated (alternating) current in response to a small-amplitude (mV order) modulated voltage stimulus. The experimental results are described based on equivalent circuits. Interpretation of impedance responses of PVSK solar cells is challenging and has not been completely resolved yet [26, 130]. Several IS studies correlated with other techniques and supported by simulations reveals that fluctuations (or hysteresis phenomena) in device performance under working conditions are related to the movements of ions and vacancies (feasibility in Li-ion battery application was also demonstrated [137-139]) that can be activated by temperature or electric field [81, 128, 135, 140-144]. A comprehensive dynamical process taking place at TiO_2/PVSK interface was described by Hu et al. [128]. Ion movement alone is not sufficient to cause hysteresis. It is the slow (~milliseconds up to minutes [81]) accumulation of mobile ions at the interfaces that leads to the dynamical hysteresis response. In the particular case, when the device is under illumination and set at V_{oc}, significant migration of positive ions and vacancies occurs at the TiO_2/PVSK interface (figure 7b) [145]. As a consequence, this leads to an upward band bending [130] signifying an energy barrier hindering electron transfer from PVSK to TiO_2 (figure 7b). It has been reported that under short-circuit conditions the ion migration is suppressed, which corroborates with PL studies [37, 52, 134] (figure 3). Garrett et al. [146] showed that when a perovskite device is illuminated, the splitting of the quasi-Fermi levels for electrons and holes take place, which is proportional to the Voc of the solar cell. I.e., a built-in potential is generated within the solar cell device that will favor migration of *charged* ions (e.g. MA^+, Pb^{2+}, I^-). On the other hand, under short-circuit conditions, the photo-generated carriers do not accumulate at the layers as they exit to the external circuit resulting in negligible built-in electric field. The dependence of this ionic motion on an externally applied electric field was further studied by Li et al. [134] employing PL mapping. The local perovskite stoichiometric variations due to external electric field (threshold > ~10^5 V/m) was shown to have a significant impact on the local PL performance. To allow ions and vacancies to build up at interfaces (that will lead to changes in the electric field distribution in the bulk PVSK),

the illuminated devices should be under the electric field under one of the following conditions: constant (i) Voc, (ii) MPP, or (iii) during J-V scan with scan rates that allow ion accumulation at interfaces [82, 130, 147, 148]. The hysteresis phenomenon, characterized by a large loss in FF (that can be followed also in Jsc and Voc) during the reverse-to-forward (R-F) scan [149, 150], has been further complicated recently by the emergence of an *inverted* hysteresis phenomenon [127, 151, 152]. Inverted hysteresis leads to reduction in J_{sc} and FF (S-shaped kink) in the F-R scans compared to that of R-F scans. Complete band diagrams for explaining normal and inverted hysteresis (NH and IH) were proposed [127] (figure 7c). Time-evolution of band diagrams within PVSK solar cells for explaining the hysteresis behavior were also proposed in figure 5 of ref. [142], Scheme 1 of ref. [140], and figure 2 of ref. [133]. A general consensus is still lacking on why inverted structured perovskite solar cells show reduced hysteresis phenomena [153-159]. Calado et al. [153] provided a comprehensible side-by-side comparison of transient optoelectronic measurements on (i) inverted device structure of ITO/PEDOT:PSS/$CH_3NH_3PbI_3$/PCBM/Al and (ii) regular device structure of n-i-p with FTO/TiO_2/$CH_3NH_3PbI_3$/spiro-OMeTAD/Au perovskite solar cells. The conclusions from this work were (i) both ion migration leading to ion accumulation at interfaces and interfacial recombination are required for hysteresis to be observed; (ii) However, they quoted that their "observation is not consistent with the hypothesis that PCBM reduces hysteresis by preventing diffusion of ionic defects, as suggested in previous works [54, 154, 155]." In addition to ion migration described above, charge trapping and detrapping at interfaces of electron and hole transport layers by the unbalanced electron and hole flux, respectively, were emphasized as possible origin of hysteresis [156]. In the particular case of ITO/PEDOT:PSS/$CH_3NH_3PbI_3$/PCBM/Al inverted planar device structure, the hysteresis is less pronounced because the electrical conductivity of PCBM (0.016 mS $\cdot s^{-1}$) is well matched to that of PEDOT:PSS (0.014 mS$\cdot s^{-1}$) [157]. The recent work by Li et al. [158] showed further the complexity of the hysteresis that can be also originated from extrinsic ion migration in perovskite solar cells. They described that not only the intrinsic ions (e.g. MA^+, Pb^{2+}, I^-) migrating within a perovskite solar cell, but also the extrinsic ions (e.g. Li^+, H^+, Na^+) originating from the contact layers (e.g., spiro-MeOTAD) have strong impact on performance and hysteresis phenomena. The above descriptions, point out that the cause for hysteresis phenomena originates from multiple physico-chemical dynamical processes taking place within the perovskite solar cell structure. Hysteresis phenomena is considered a serious impediment to stabilized and reliable measurement and operation of the perovskite solar cells.

Furthermore, moving ions in the bulk of PVSK was also suggested to play major role in the degradation of the device, which are all important issues to be considered towards application [128, 136, 141, 160, 161].

4. Up-scaling strategies

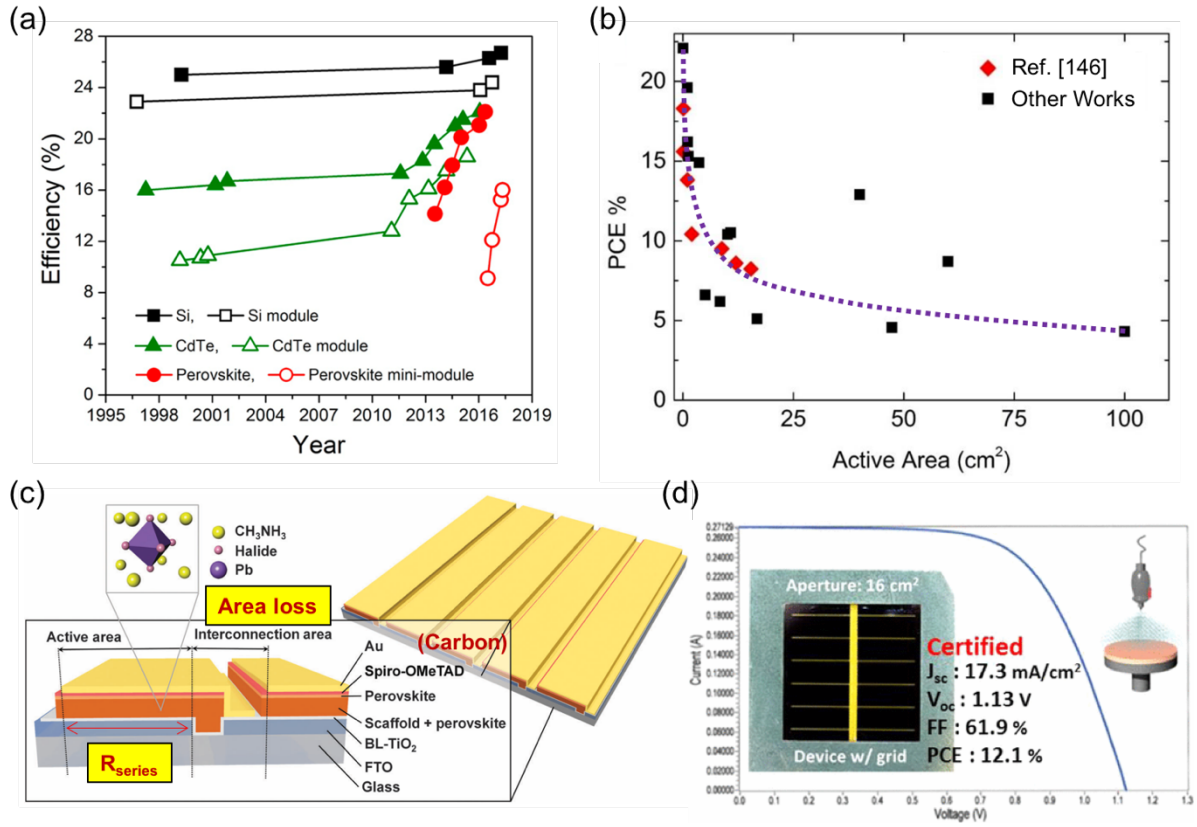

Figure 8. (a) Efficiency evolution of Si, CdTe, and PVSK single cells and modules (or mini-modules) in the past 20 years. (b) Reported module efficiencies as a function of active area measured by J-V curves. (c) Schematic drawing showing the structure of a typical PVSK solar module. (d) Devices with metal grid help overcome the series resistance (R_{series}). Certified efficiency (Newport, August 30th, 2016) (a) Reprinted with permission from ref. [162]. Copyright 2017 American Chemical Society. (b) Reprinted with permission from ref. [163]. Copyright 2016 The Royal Society of Chemistry. (c) Reprinted with permission from ref. [164]. Copyright 2015 The Royal Society of Chemistry. (d) Reprinted with permission from ref. [165]. Copyright 2017 American Chemical Society.

PVSK synthesis has evolved significantly and, as a result, a variety of PVSK compositions can be obtained [11, 18, 22, 166-173]. In addition to thin-films, single crystals

of these materials were synthesized and used in devices [90, 174-183]. However, the current state-of-the-art perovskite single cells have relatively small active areas (<0.3 cm^2) [10, 11, 22, 83, 87, 166-169, 184-186], which is impractical for realistic applications [6, 7, 162]. Therefore, it is imperative to develop up-scaling processes with high PCEs and good stability. The number of reports on PVSK single cells employing active areas larger than 1 cm^2 is not many, but certainly increasing [187-192]. An area of 1 cm^2 can only be considered an "intermediate size" in solar cell industrial standards. Therefore, further up-scaling of PVSK solar modules is desirable, and we have seen more and more studies focusing on this topic (figure 8a) [11, 157, 162, 163, 165, 193-204]. As we can see from the comparison of PVSK PVs, single crystalline Si and polycrystalline CdTe PV technologies, the progress reported for PVSK PV modules (or mini-modules) are also advancing faster than other PV technologies [162]. One of the major challenges in PVSK solar modules is that the module efficiency decays as the active area of a solar module rises (figure 8b) [163, 191]. When scaling up to larger areas, the performance reduction is usually a result of decreased FF and J_{sc}. The decrease in FF is associated with the increase in series resistance (R_{series}) due to a longer transport distance through the transparent conductive oxide (TCO), which typically has small, but finite sheet resistance range of 10~15 Ω/□ (figure 8c). This is an important issue, and can be improved with optimized module design. For example, fabricating narrower cells reduces the travel distance through TCO, and thus lowers R_{series}. However, the narrowing of the active area cells will lead to increase in the interconnection areas (figure 8c), and therefore decrease the percentage of active area for a given total area leading to increased cost of generated solar electricity (i.e., a higher $/W value). In these interconnection areas, no electricity is being generated leading to a further decrease in PCE when normalized by the total substrate area. It is important to keep in mind that PCE per total area is more relevant for practical applications than PCE per active area (figure 8c). Often a geometric fill factor (GFF = active area / total area) is used to quantity solar module area usage efficacy [205]. An alternative design for large-area single cell is based on utilizing metal grids (similar design employed in Si solar cells) that is effective in reducing R_{series} issues (figure 8d) [165]. The decrease in J_{sc} upon up-scaling is often related to deteriorated PVSK film quality and uniformity when the substrate area becomes larger. Development of fabrication techniques that can generate high quality uniform PVSK film across large areas relies on (i) a priori understanding of complex nucleation and growth processes of PVSK films [206, 207], (ii) perovskite film deposition methods (solution process or vacuum deposition) with a high degree of controllability to ensure low cell-to-cell and batch-to-batch variation, and (iii) a posteriori

spatially resolved chemical composition distribution and morphology characterization of the entire perovskite films as well as when incorporated in complete devices.

Monitoring perovskite film quality during spin coating was achieved by *in situ* time resolved grazing incidence wide angle X-ray scattering (GIWAXS) measurements [208, 209] to investigate the origins of detrimental effects of incomplete lead precursor conversion, inconsistent crystallite formation/film uniformity, and precursor-solvent coordination [207]. In addition, characterization techniques such as electroluminescence (EL) and PL imaging and light induced current measurements (LBIC) of the complete cell was shown to be helpful to visualize non-local homogeneities and identify spatially present defects and/or (dust) particulates that lead to shunting pathways [165, 210-218]. Fundamental principles of local radiative/non-radiative charge recombination and charge transport in solar cells are addressed with above techniques. For example, in figure 9b, dark spots delimited by square are cell areas limited by series resistances (R_{series}). A larger hole marked by triangle is a poorly contacted region due to processing defects. Cells are defined by the circle is a well contacted region with high radiative recombination [217]. Compositional uniformity is equally important for obtaining high performance cells, and X-ray fluorescence (XRF) and Rutherford backscattering spectroscopy (RBS) have been used to provide vital information regarding compositional uniformity [193]. Considering up-scaling, the first step is fabrication of large-area perovskite solar cells with high quality (i.e., high film uniformity, reduced roughness across the whole area, reduced density of defects, etc.). In this aspect, the methods are currently under intensive investigation include (i) methylamine-gas treatment (and its variants) (figure 9e,f) [8, 129, 219-229], (ii) vapor based methods including vacuum evaporation [9, 83, 230-235] and chemical vapor deposition [163, 236-239], and (iii) preferentially oriented crystal growth (figure 9g) [240-245]. For instance, it has been demonstrated that certain crystallographic orientations of perovskites grains can lead to enhancement in carrier mobility and impact significantly the V_{oc} and PCE [240]. CVD is a mature technique, which has been widely employed in many industrial applications. Perovskite film growth by a hybrid chemical vapor deposition (H-CVD) process for the fabrication of PVSK solar cells was first demonstrated in 2014 [238]. Later, the H-CVD process has been shown to have a high level of controllability for film morphology and composition [163, 195, 236-239, 246-251]. The H-CVD method consists of two steps. In the first step, $PbCl_2$ (or PbI_2) films are deposited to the substrates via vacuum evaporation or solution processing (figure 10a) [238]. In the second step, these substrates pre-coated with $PbCl_2$ (or PbI_2) films are placed in the low temperature zone of a two-zone tube furnace. A crucible containing MAI (or FAI) is placed in the high

temperature zone of the tube furnace. When the high temperature zone is heated up, MAI (or FAI) becomes vapor. A dry N_2 gas flow is used to drive the MAI (or FAI) vapor from the high temperature zone towards the low temperature zone, where MAI (or FAI) is deposited on $PbCl_2$ (or PbI_2) and converts the film to perovskite. During the CVD process, the pressure inside the tube furnace is kept at a rough vacuum level (approximately 100 Pa). The H-CVD (figure 10a) method does not have the solvent compatibility issues, which are often encountered in solution processing. The solution-free feature of the H-CVD method means that it can be conveniently integrated with Si, CIGS and CdTe solar cells to form tandem cells. It has also been shown that uniform films across large areas can be prepared by the H-CVD method, which is fully compatible with high-throughput production (figure 10b) [163, 236-239]. Furthermore, when scaled up from 0.1 cm^2 small cell to 12 cm^2 module, the PCE has only slightly dropped from 16.6% to 14.6% (figure 10c) [239]. These studies suggest that the H-CVD method is a promising method that is compatible to up-scale the fabrication of PVSK solar cells (figure 10c). Although much progress has been made, there is still plenty of work to be done to achieve large-area perovskite solar cells. Once the first step of fabricating a homogeneous and densely packed PVSK film over a large area is realized, it can be followed by the second step of design and fabrication of a module and the third step of integrating the modules into a panel [7, 163, 194].

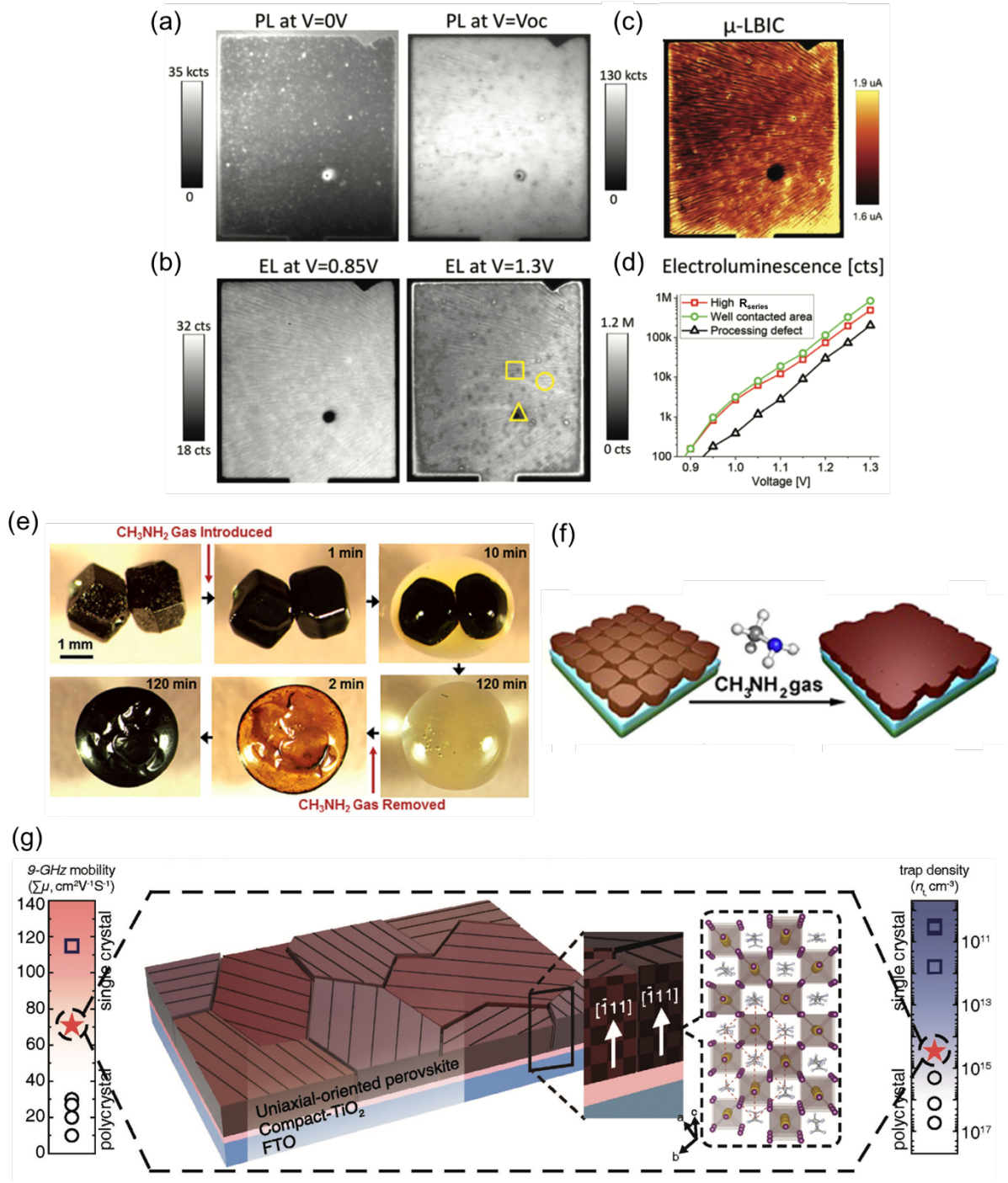

Figure 9. (a) Photoluminescence (PL), (b) Electroluminescence (EL) mapping at I_{sc} and V_{oc} conditions. (c) Micro light induced current (μ-LBIC) measurements measured at 532 nm. (d) Voltage dependent local electroluminescence emission from the regions marked in the EL image at 1.3 V. (e) In situ optical microscopy of the morphology evolution of $MAPbI_3$ perovskite crystals upon exposure to CH_3NH_2 (MA) gas and subsequent degassing. (f) The utilization of MA-gas treatment to "*heal*" PVSK thin-films prepared by other fabrication methods. In this example, the MA-gas treatment improves the morphology, crystallinity, and optical and charge transport properties of perovskite films prepared by methylamine post-

annealing method [219]. (g) Schematic of the uniaxial-oriented PVKS films. Carrier mobility and trap density of [−111] uniaxial-oriented PVSK films (red stars) are also represented with previous reported values from polycrystalline (open circles) and single-crystal (open squares) PVSKs. (a-d) Reprinted with permission from ref. [217]. Copyright 2015 The Royal Society of Chemistry. (e) Reprinted with permission from ref. [223]. Copyright 2015 WILEY-VCH Verlag GmbH & Co. KGaA, Weinheim. (f) Reprinted with permission from ref. [8]. Copyright 2017 WILEY-VCH Verlag GmbH & Co. KGaA, Weinheim. (g) Reprinted with permission from ref. [240]. Copyright 2017 WILEY-VCH Verlag GmbH & Co. KGaA, Weinheim.

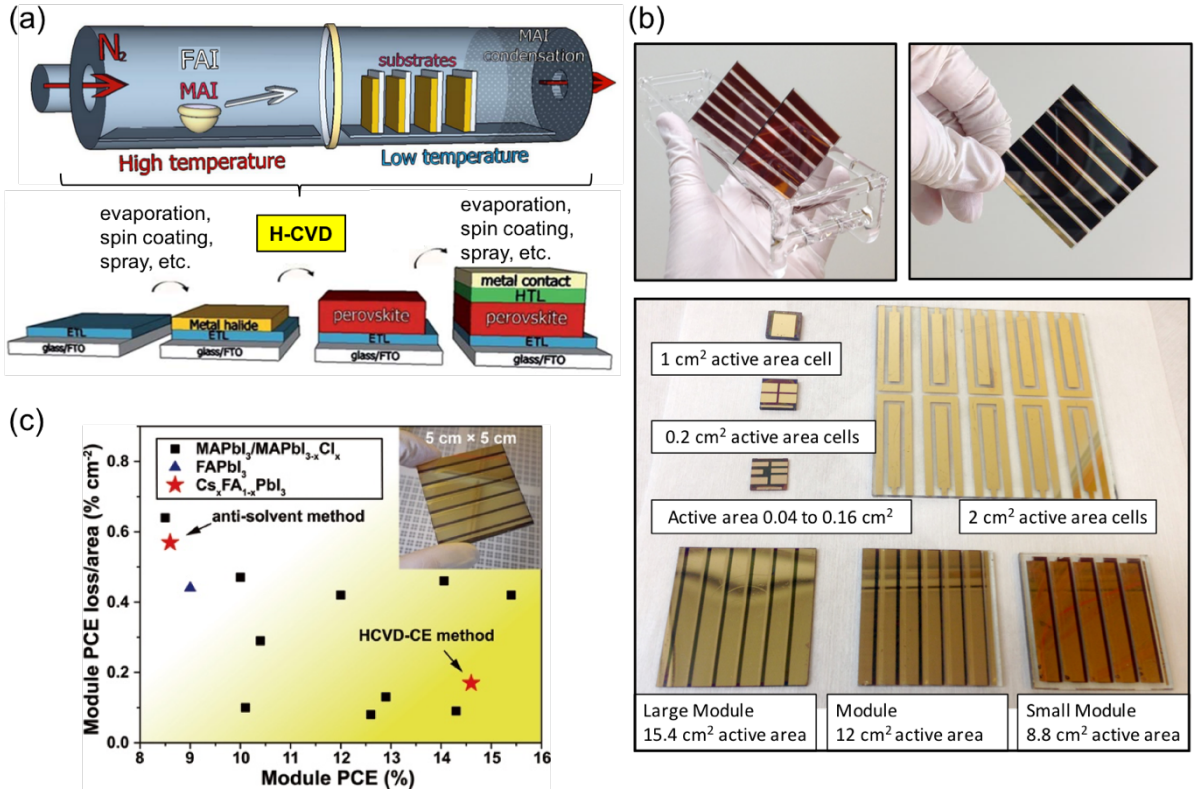

Figure 10. (a) Schematic of the H-CVD method for uniform perovskite film deposition across large areas. Details are provided in ref. [238]. (b) Photographs of patterned PVSK films grown by H-CVD and solar cells and modules. (c) Combined H-CVD and cation exchange (CE) to up-scale the fabrication of Cs-substituted mixed cation PVSK solar cells with high efficiency and stability. (a) Reprinted with permission from ref. [238]. Copyright 2014 The Royal Society of Chemistry. (b) Reprinted with permission from ref. [163]. Copyright 2016 The Royal Society of Chemistry. (c) Reprinted with permission from ref. [239]. Copyright 2017 WILEY-VCH Verlag GmbH & Co. KGaA, Weinheim.

5. Long-term Stability

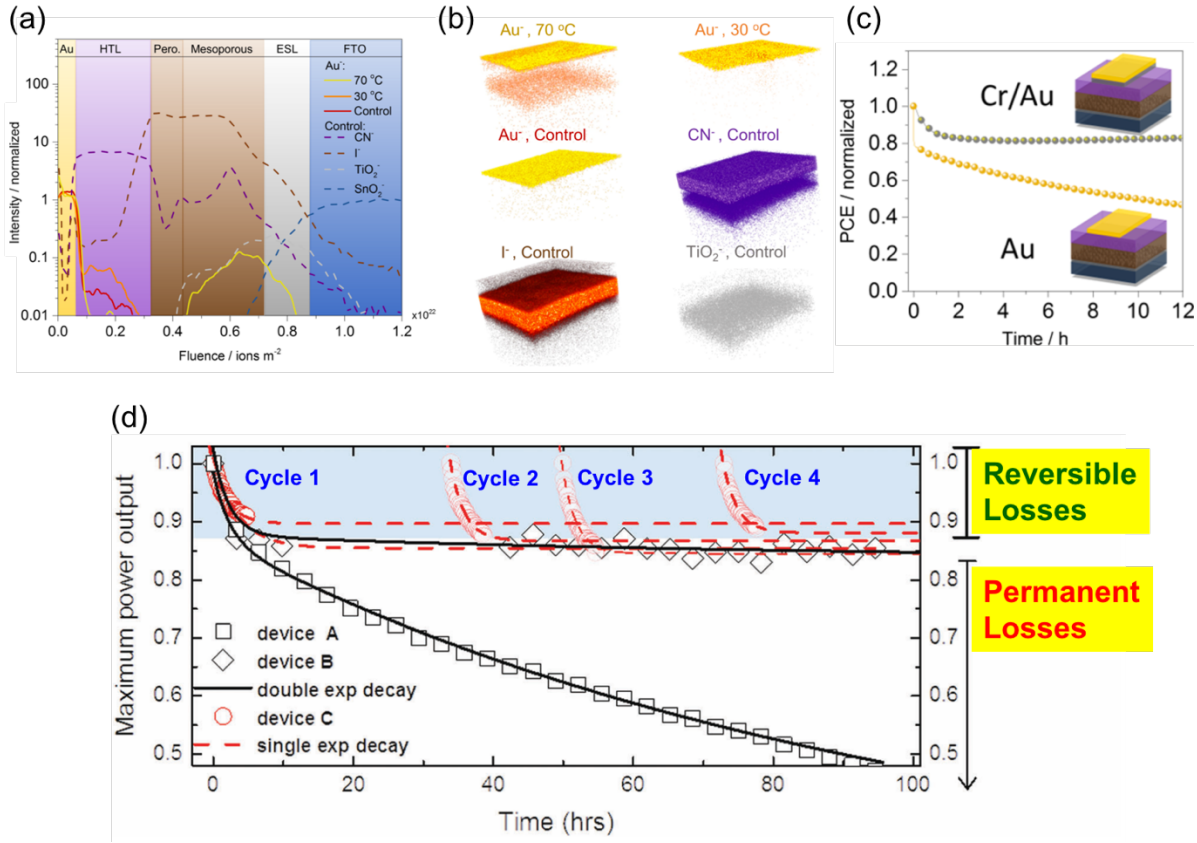

Figure 11. (a) Time-of-flight secondary ion mass spectrometry (ToF-SIMS) depth profiles of degraded PVSK solar cells. Profile of Au^- is compared to that of the devices aged at 30 °C and 70 °C. (b) Reconstructed elemental 3D maps for the ion traces in the depth profile. The xy dimensions of the analyzed area is 10 × 10 μm^2. (c) MPP tracking aging (under 1 sun at 75 °C and N_2 flow) of PVSK solar cells with top HTL/Au and HTL/Cr/Au layers. The values are normalized to the initial ones. (d) Normalized maximum power output (V ~ 0.85 V) tested in N_2 environment for 3 identically prepared perovskite solar cells (devices A, B, C) measured under 1 sun. Devices A and B were continuously tracked for over 100 h. Device C was cyclically tracked 4 times for 5 hours and it was left in dark at open circuit between consecutive measurements. (a-c) Reprinted with permission from ref. [252]. Copyright 2016 American Chemical Society. (d) Reprinted with permission from ref. [82]. Copyright 2017 The Royal Society of Chemistry.

In addition to the series resistance issue of TCO (figure 8) and thin-film quality when considering up-scaling (figure 9), a third factor that leads to dramatic irreversible PCE decrease over time is correlated with the temperature increase (60 ~ 85 °C) in large area solar modules under 1 sun. [163, 253-255]. Demonstration of solar modules operating successfully under

operation conditions (i.e., under light and connected with a load) and thermal stress testing (-40 ^{o}C and 85 ^{o}C) is needed to obtain industrially relevant certification (IEC61646 / IEC61215 protocol) [7, 205, 253, 256, 257]. A number of reports have shown that it is unlikely for $MAPbI_3$ based solar cells to reach sufficient stability as $MAPbI_3$ (i) undergoes a phase transition from tetragonal to cubic phase at approximately 57 °C [163, 258], which is followed by significant increase in charge-carrier trapping rates upon entry into the cubic phase [259] and interfacial recombination rates increase at the interfaces between the selective contacts and the $MAPbI_3$ layer [260-262], (ii) possesses low decomposition temperature [263], (iii) organic cation sublimes from PVSK and decompose at solar cell operation temperatures [264-266], (iv) extreme sensitivity to atmospheric conditions [132, 253, 267-270], (v) generation of I_2 leading to subsequent migration and subsequent neighbor degradation (cascade effect decomposition) [271-273]. More recently, as shown in figure 5, alloying of perovskites was shown as an effective strategy to improve stability [18, 22, 274]. In fact, except for the first certified efficiency record reported for PVSK cells using pure $MAPbI_3$ [166], the following subsequent five National Renewable Energy Laboratory (NREL) records with publicly disclosed information employed mixed-cation and mixed-halide PVSK strategies showing both enhanced efficiency and stability [11, 18, 22, 167-170]. The overall degradation within a PVSK solar cell is not solely originated from the PVSK layer, but also can result from adjacent layers as well as interface related degradation issues [7, 14, 77, 132, 253, 269, 275-284]. As shown in figure 5, the best-performing PVSK solar cells share a common device structure composed of FTO/c-TiO_2+mp-TiO_2/PVSK/organic based HTL/Au. Among several alternative ETLs studied [285-287], combination of c-TiO_2 and mp-TiO_2 employed as ETL leads to high PCEs as well as reduced hysteresis. However, TiO_2 was associated with photocatalytic degradation processes at the TiO_2/PVSK interface upon UV light illumination [281, 288]. Furthermore, although great efforts have been made in developing alternative HTLs [14, 289-294], LiTFSI-doped spiro-MeOTAD generally gives higher solar cell device efficiencies [14]. But it has been reported that the spin coated LiTFSI-doped spiro-MeOTAD HTL (i) contains pinholes [14, 294-297], (ii) dynamics of dopants strongly affects HTL conductivity [14, 295, 298, 299], and (iii) the hygroscopic nature hampers overall device stability [14, 277, 290, 291]. The top cathode is generally noble metal Au with good air stability, but it has been also associated with long-term thermal stability issues at high temperatures because Au in the form of clusters/atoms diffuses through the spiro-MeOTAD HTL reaching the PVSK layer (figure 11a-c) [252]. As shown in figure 4d and figure 11d and described in references [55, 82], mild

operation conditions (i.e., determination of device characteristics) that allow *self-healing* of device itself [300-302] are proposed to alleviate the short lifetime of PVSK-based solar cells. Note that self-healing materials [300, 303] are under investigation in other solar cell technology [301, 302]. For example, polymers [e.g., polyvinyl alcohol (PVA), polyurethane, poly(methyl methacrylate) (PMMA), etc.] often employed as encapsulation materials are susceptible to degradation and crack formation upon prolonged light exposure. Polyisobutylene (PIB) based sealant was introduced as the encapsulant in organic electronics. Interestingly, PIB based networks show the *light-induced self-healing* properties that leads to longer polymer lifetime and thus, prolonged device stability [301, 302]. In the PVSK solar cell research, Zhao et al. reported the first PVSK device study with *self-healing* properties employing polyethylene glycol (PEG) as the scaffold (polymer) layer into which PVSK is infiltrated [304]. These PEG molecules in close contact with PVSK crystals effectively absorb water leading to prolonged PVSK crystals. The self-healing mechanism was illustrated: upon water vapor (60 s), the PEG+PVSK film turned to yellow color at first, but recovered to the black color material within 45 s after removal of water vapor. In contrast, the PVSK film without PEG turned yellow in an irreversible manner [304]. There are a few reports that demonstrated the feasibility to obtain long-term stability in PVSK based solar cells taking into to account strategic device designs. For example, the device with the structure FTO/c-TiO_2/m-TiO_2/$Rb_{0.05}Cs_{0.05}(FA_{0.83}MA_{0.17})_{0.90}Pb(I_{0.83}Br_{0.17})_3$/PTAA/Au showed high steady-state PCE of 21.6%. More importantly, these cells were demonstrated to maintain ~95% of their initial PCE when tested in N_2 at a temperature of 85 ^oC for 500 h and under operation conditions [47]. In another study, the device with the structure FTO/SnO_2/C60/$Cs_{0.17}FA_{0.83}Pb(I_{0.6}Br_{0.4})_3$/spiro-OMeTAD/Au not only achieved an efficiency as high as 18.3%, but also showed enhanced stability with a post burn-in T80 over 3,420 hours under continuous 1 sun illumination in air [305]. In addition to strategic designs of PVSK materials, encapsulation strategies should be also employed in the current PVSK solar cell research to achieve long term stability [7, 189, 205, 253, 306]. For example, $FA_{0.83}Cs_{0.17}Pb(I_{0.83}Br_{0.17})_3$ based PVSK solar cells that were packed with top glass sheet employing EVA (polymer binder) and butyl rubber as edge sealant demonstrated unprecedented stability (figure 12a-e) [189, 253]. These PVSK single cells were demonstrated to pass the most difficult IEC test of damp heat, i.e., 1000 h at 85 ^oC and 85% relative humidity (RH) (figure 12e). Another impressive example of feasibility in obtaining long term stability (one-year) was based on the 2D/3D mixed PVSK structure of $(HOOC(CH_2)_4NH_3)_2PbI_4$ (AVAI) / $MAPbI_3$ with top carbon electrode (figure 12f-h) [205]. The champion cell (0.64 cm^2, active area) and module (47.6 cm^2, active area; GFF = 47.6%)

delivered PCE of 12.7% and 11.2%, respectively. The results in figure 12h show impressive long-term stability of >10,000 h and minimum influence at elevated temperatures. This long stability report is at present the highest record value obtained in PVSK PVs, demonstrating the proof-of-concept that careful selection of PVSK composition/structure allows conventional encapsulation to adequately protect PVSK and lead to long-term stability [189, 205, 253]. These new advances are encouraging for PVSK solar cells.

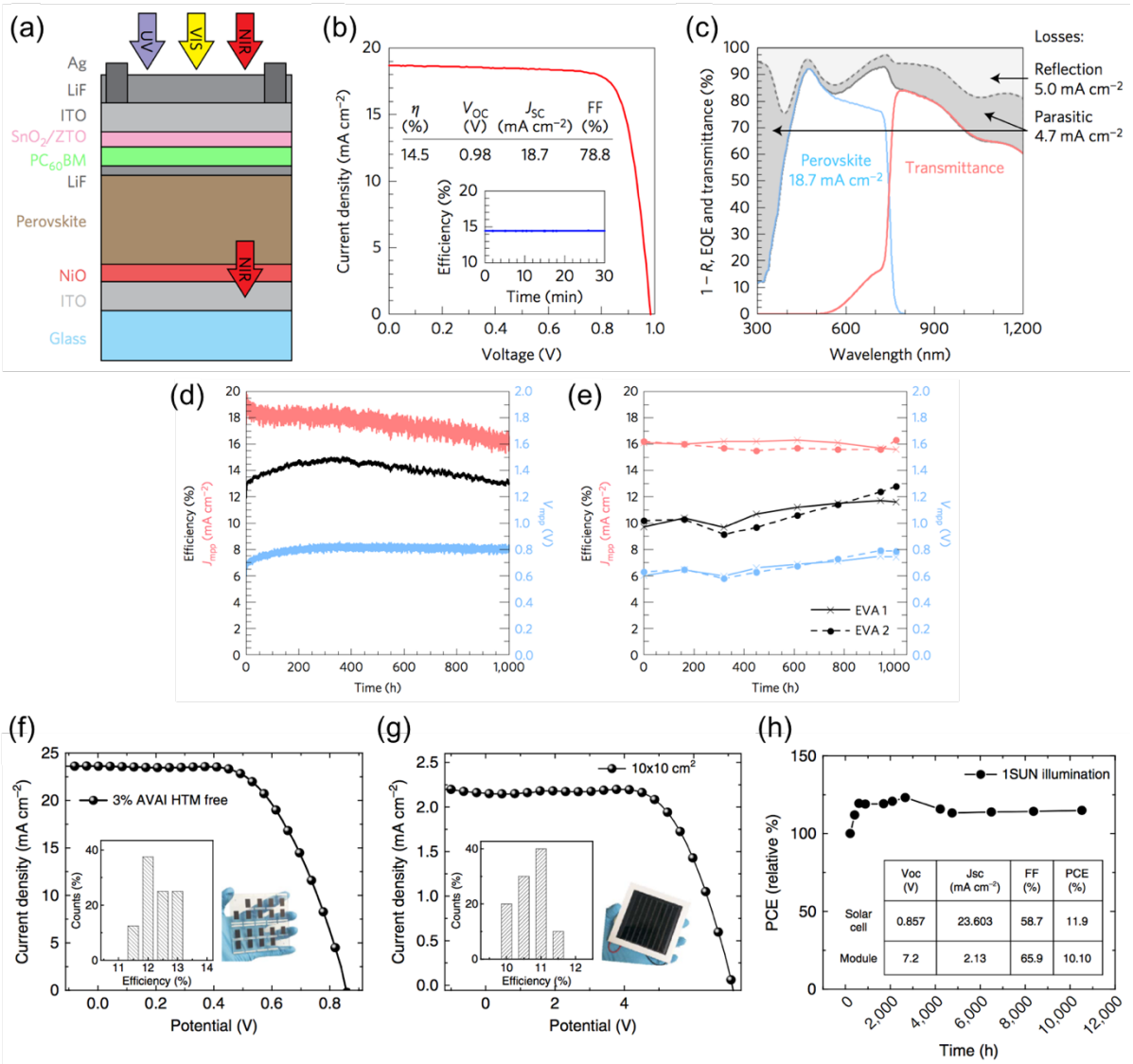

Figure 12. (a) Solar cells based on $FA_{0.83}Cs_{0.17}Pb(I_{0.83}Br_{0.17})_3$ PVSK with a band gap of 1.63 eV. These cells were later combined with silicon solar cells to make a monolithic tandem solar cell delivered NREL certified and record 23.6% PCE. (b) J-V characteristics and (c) total absorbance (1 − R, where R is the reflectance; dashed grey line), EQE (solid blue line), and transmittance (solid red line). The light and dark grey shaded areas represent the light lost to reflection and parasitic absorption, respectively; associated current density losses are indicated.

(d) Efficiency, J_{MPP}, and V_{MPP} of a PVSK device with no additional encapsulation during 1,000 h of continuous MPP tracking. (e) Efficiency, J_{MPP}, and V_{MPP} of PVSK device packaged with EVA, glass, and a butyl rubber edge seal for damp heat testing (85 ^{o}C / 85% RH, IEC protocol 61215). (f) J-V of encapsulated 2D/3D AVAI/$MAPbI_3$ based PVSK solar cells (0.64 cm^2) and (g) solar modules (47.6 cm^2) with carbon electrode. (h) Stability measurement of solar module tested under 1 sun at stabilized temperature of 55 ^{o}C and J_{sc} condition. (a-e) Reprinted with permission from ref. [189]. Copyright 2017 MacMillan Publishers Limited. (f-g) Reprinted with permission from ref. [205]. Copyright 2017 MacMillan Publishers Limited.

6. Lead toxicity

Pb^{2+} toxicity is another major obstacle for high efficiency Pb-based PVSK solar cells to go towards commercialization. The PV community is aware of the consequences of Pb toxicity and the anxiety that poses for the society [7, 307-311]. The structural and electronic properties of Pb-halide-based PVSKs are extremely suitable for solar energy harvesting applications, and it is therefore not easy to find a replacement for Pb. So far, only Sn-based PVSK solar cells have produced reasonable PCEs (the highest PCE of 8.12% was achieved on $FA_{0.75}MA_{0.25}SnI_3$-based solar cells [312]). Till now all other Ge-, Cu-, Sn-, Bi-, and Sb-based PVSKs have yielded relatively low PCEs (Refs. [313-315] summarize comprehensively the reported efficiencies for Pb-free PVSK solar cells). Density functional theory (DFT) calculations confirm that the electronic configuration of Pb^{2+} in PVSK is one of the key reasons responsible for the exceptional PV behavior [70, 308, 316, 317]. The so-called inert *s* pair (2+ oxidation state is stabilized in group IV elements when electrons in s^2 pair are kept intact and only *p* electrons are lost) is preferred in heavier atoms such as Pb due to stabilized *s* orbitals by relativistic contraction. As a consequence, Pb is stable in 2+ state while as the most stable oxidation state for Sn or Ge (located above Pb) is 4+.

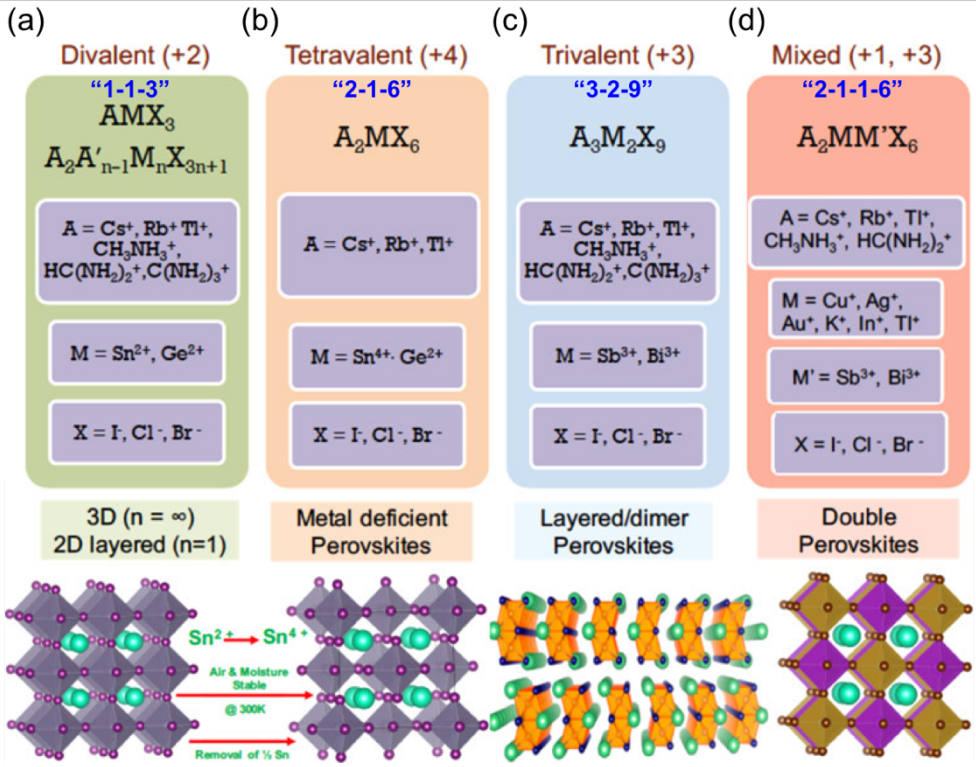

Figure 13. Reported PVSK structures of (a) AMX_3 or "1-1-3" 3D structure (e.g. $CH_3NH_3PbI_3$); (b) A_2MX_6 3D structure; (c) $A_3M_2X_9$ or "3-2-9" with lower-dimensionality structure (e.g. $Cs_3Bi_2I_9$); and (d) $A_2MM'X_6$ or "2-1-1-6" chess-type structure (e.g. $Cs_2AgBiBr_6$). Reprinted with permission from ref. [314]. Copyright 2017 American Chemical Society.

Seeing that a simple Pb^{2+} substitution by another divalent element in the AMX_3 or "1-1-3" (3D) structure (figure 13a) is challenging, efforts are being made to search for multivalent elements yielding "2-1-6" (3D) structure (figure 13b), "3-2-9" bilayer (2D) [318-325] (figure 13c), bioctahedra (0D), "3-1-5" single-chain, "4-1-6" single-octahedron structures, and "2-1-1-6" (3D) double perovskite structure with compensated charges (figure 13d) [317, 326-332]. The size, shape, and functionality of organic cations alter the 3D inorganic network to form extended 2D layers, 1D chains, 0D isolated octahedra or other intermediate cases [333]. In a recent work, Xiao et al. [317] compiled reported Pb-free halide perovskites and non-perovskites with a wide range of bandgaps and correlated with structural dimensionality. The term non-perovskites correspond to structures consisting of non-corner-sharing or isolated $[MX_6]$ octahedra. Although most of the reported bandgap values correlate well with the structural dimensionality, the same authors introduced the concept of electronic dimensionality, which is associated with the charge transport of photogenerated carriers. Higher electronic dimensionality accounting for better photovoltaic device performances is

associated with isotropic (3D) transport properties, with smaller recombination events in well-ordered 3D structured absorber [317]. This electronically dimensionality was associated with the generally lower power conversion efficiencies observed employing lower dimensional PVSKs: $Cs_3Bi_2I_9$ (2.2 eV E_g, 1.09% PCE) [318], $MA_3Bi_2I_9$ (2.26 eV E_g, 1.64% PCE) [325], $Rb_3Sb_2I_9$ (2.24 eV E_g, 0.66% PCE) [322].

The atomic transmutation strategy ($2M^{2+} \rightarrow M_1^{+} + M_2^{3+}$) has led to successful evolution of a binary ZnSe (E_g = 2.8 eV) to ternary $CuGaSe_2$ (E_g = 1.7 eV), and then to quaternary $Cu_2ZnSnSe_4$ (E_g = 1 eV) [332, 334-336]. These $CuGaSe_2$ and $Cu_2ZnSnSe_4$ based compounds led to further development of $Cu(In,Ga)Se_2$ (CIGS) and Cu_2ZnSnS_4 (CZTS) that have been applied in solar cells reaching PCEs above 20% and 10%, respectively [10]. The same transmutation strategy is being explored in PVSKs towards a novel class of Pb-free quaternary materials with $A_2MM'X_6$ or "2-1-1-6" 3D double-PVSK structure (figure 13d). Metals with oxidation states of 2+/2+ and 1+/3+ in the M/M' sites can be accommodated in double perovskites. Although their PCEs have not been reported, some examples of compounds promising for photovoltaic applications include: $Cs_2Ag^{1+}Bi^{3+}X_6$ (X = Br and Cl) [326, 327, 334, 337], Cs_2NaBiI_6 [317], $Cs_2InAgCl_6$ [338], Cs_2InBiX_6 (X = Br and Cl) [334], $(MA)_2AgBiBr_6$ [339], and $(MA)_2KBiCl_6$ [328]. Computational screening procedures are helpful in searching for new structurally stable double perovskites [329, 332, 340, 341]. Volonakis et al. proposed a new family of Pb-free inorganic halide double perovskites $A_2B'B''X_6$ based on A = Cs, B' = Au, Ag, Cu, B" = Bi or Sb, and X = Cl, Br, I using first-principle calculations that exhibit promising optoelectronic properties. So far, working solar cells based on double perovskites have not been reported to date. This has been majorly attributed to difficulties in developing synthetic routes to obtain uniform thin films of the correct phase and composition [317, 329-331, 334].

Recently, PVSKs have also gained attention as suitable materials for γ-ray [342, 343] and X-ray detectors [344-346] as well as X-ray imaging systems [347, 348]. X-ray detectors employing Pb-based PVSKs (thin-films and single crystals) were reported to achieve high sensitivities outperforming commercial α-Se X-ray detectors [337], which are of great potential for a range of applications such as medical diagnosis – operating at low X-ray doses to reduce health risks caused by radiation [347, 348]. Employing the atomic transmutation method ($2Pb^{2+} \rightarrow Ag^{+} + Bi^{3+}$) in the $CsPbBr_3$ PVSK (shows enhanced stability), the double PVSK structure $Cs_2AgBiBr_6$ was first introduced in X-ray detector devices [337]. Pb-free

$Cs_2AgBiBr_6$ based X-ray detectors showed a low detectable dose rate limit that was comparable to the $MAPbBr_3$ single crystal [337].

7. Summary and Outlook

PVSK solar cells with efficiencies as high as 22.7%, are currently the only solution-processable PV technology that demonstrated potential to outperform multicrystalline Si (21.9%) and be competitive with emerging thin-film solar cells such as vacuum-processed CIGS (22.6%) and CdTe (22.1%) [10]. Currently there are three main challenges for PVSK solar cells: (i) most of these high PCE values were obtained in small active areas, and (ii) the lifetime of these cells is relatively short, and (iii) these cells are mainly based on Pb-based PVSKs. These challenges on the other hand also point out the new directions in the PVSK research [6, 349, 350]. Challenge (i) has been discussed in detail in section 4, which includes two issues impeding the fabrication of large-area efficient PVSK solar cells and modules. The first issue is the deterioration in PVSK film morphology and uniformity when the cell or module areas become larger. The second issue is the inherent increase in R_{series} of TCO when increasing the cell or module area. In 2015, the largest reported PVSK solar cell had an active area of 100 cm^2 and generated a PCE of 4.3% (429 mW) and V_{oc} of 9.6 V [197]. In 2016, PVSK solar modules fabricated using a full dry process of H-CVD was demonstrated (figure 10); $FAPbI_3$-based modules with PCE up to 9% (6-cell modules; 12 cm^2 active area) were reported [163]. In 2017, several studies focusing on perovskite solar modules have been reported representing state-of-the-art in this direction: PCE of 10.4% (49 cm^2 active area) [194], certified PCEs of 12.1% (36.1 cm^2 aperture area) [187], 12.1% (16 cm^2 aperture area; but employing metal grid strategy) [165], and 15.76% (6×6 cm^2 total area; 20 cm^2 active area) [351]. Currently, the best certified perovskite mini-module efficiency of 16% has an aperture area of 16.29 cm^2 [11]. These reports show that large-area PVSK solar modules can be realized. As comparison (and also a further motivation for the PVSK community) monocrystalline Si cell was also demonstrated this year to achieve PCE of 26.3% with an area of >180 cm^2 [20, 21]. Challenge (ii) is regarding long-term stability (e.g., >20 years achievable in Si PV technology) of PVSK solar cells. Accelerated PVSK stability tests under thermal stress following IEC 61646/IEC 61215 [257] can provide vital information regarding the solar cell operational stability. As discussed in section 5, a proper selection of PVSK composition/structure (e.g., mixed cations, mixed anions, and 2D/3D mixed PVSKs) with the

additional encapsulation strategy was demonstrated to lead to one-year long stable operation [189, 205]. Further investigations are needed regarding the influences of concentrated sunlight (e.g., 100 suns = 10,000 mW/cm^2) in PVSK materials [352-355]. However, accelerated stability test protocols (e.g., under 100 suns and MPP tracking) are expected to be more practical and boost up the research outcomes on the stability profiles of PVSK solar cells [355]. In addition, self-healing materials have been employed in PVSK solar cell research and may be additionally a viable strategy to attain long-term stability [304]. Challenge (iii) regarding the toxicity of Pb^{2+} (section 6) most concerns investors and costumers, which has led to a new research direction, i.e., Pb-free PVSKs. Currently, Pb-free PVSK solar cells exhibit inferior performance compared to Pb-based counterparts. More research efforts are needed to develop new alternative Pb-free PVSKs, as well as to understand the main factors causing the low efficiencies in the current Pb-free PVSK cells. For example, it is necessary to explore and develop alternative ETLs and HTLs for matching energy levels and minimize charge-recombination events at interfaces (section 6) for these Pb-free PVSKs.

The outlined technological challenges above (e.g., small cell areas, instability, low efficiencies in Pb-free PVSKs) are closely correlated with fundamental bulk and interface properties within a complete solar cell device. For instance, efficient charge-carrier generation, extraction, and transport with minimum recombination through the interfaces is crucial to attain high-efficiency solar cells. Furthermore, PVSK thin-film fabrication methods generate polycrystalline grains. The adjacent grains may assume different crystal orientations and have different chemical compositions (and/or impurities), which impacts charge dynamics and thereby the overall solar cell performance. As shown in figure 5, the best performing PVSK solar cells have a complex structure comprising multiple interfaces: FTO/c-TiO_2+mp-TiO_2/PVSK/organic based HTL/Au. Efforts are being made to observe the dynamical processes taking place within the complete device under solar cell operating conditions (section 3) [356, 357]. Except for a small number of studies [80, 358], often the description of fundamental aspects in PVSK materials are based on static cases by comparing *pristine* and/or *fresh* film condition with its *after treatment* conditions (such as after an annealing treatment, gas-exposure, solar cell operation, *etc.*). For instance, (i) optical properties of perovskite films by UV-vis and PL; (ii) perovskite structural determination by XRD; (iii) valence band and conduction band energy levels determination by photoemission and inverse photoemission spectroscopy techniques [98, 106, 115]; (iv) microstructure and morphologies by scanning probe microscopy (SPM) techniques were intensively employed as characterization tools in PVSK materials with minimum external stimulus (minimized “perturbation”) during a

measurement [359, 360]. However, it is also important to evaluate how much the external environment and probing source (e.g., visible light, X-ray, bias, etc.) of an analytical tool are influencing PVSKs under measurements [135, 361]. Moving one step further, these external stimuli [362] can be even used strategically and controllably to probe a real-time dynamical process taking place in PVSK materials (figure 2b) and solar cells (figure 3). *S*ynchrotron radiation (SR) techniques have been used to study PV device dynamics under a number of different stimuli such as cooling/heating, current/voltage, light, and environmental stressing conditions (so called *in operando* measurements). *In operando* measurements were demonstrated on $CH_3NH_3PbI_3$-based solar cell by designing a sample stage for simultaneous current-voltage curves dependent measurements on temperature and SR X-ray diffraction [363]. A detailed correlation between perovskite crystal structure and current-voltage profiles were measured simultaneously on the same device sample, yielding insights into the tetragonal-to-cubic phase transition temperature (60.5 ~ 65.4 ^oC). Such *in operando* measurements shed light on the dynamics of perovskite solar cells under working conditions. The earned knowledge is expected to lead to a new wave of technological advances in PVSK solar cells.

Acknowledgements

This work was supported by funding from the Energy Materials and Surface Sciences Unit of the Okinawa Institute of Science and Technology Graduate University, the OIST R&D Cluster Research Program, the OIST Proof of Concept (POC) Program and JSPS KAKENHI Grant Number 15K17925.

ORCID

Luis K. Ono: 0000-0003-3176-1876

Yabing Qi: 0000-0002-4876-8049

References

[1] Breyer C, Bogdanov D, Gulagi A, Aghahosseini A, Barbosa L S N S, Koskinen O, Barasa M, Caldera U, Afanasyeva S, Child M, Farfan J and Vainikka P 2017 On the role of solar photovoltaics in global energy transition scenarios *Prog. Photovolt. Res. Appl.* **25** 727-45

[2] Kurtz S, Haegel N, Sinton R and Margolis R 2017 A new era for solar *Nat. Photon.* **11** 3

[3] Gul M, Kotak Y and Muneer T 2016 Review on Recent Trend of Solar Photovoltaic Technology *Energy Explor. Exploit.* **34** 485-526
[4] Ahmad S 2016 An affordable green energy source—Evolving through current developments of organic, dye sensitized, and perovskite solar cells *Int. J. Green Energy* **13** 859-906
[5] Feurer T, Reinhard P, Avancini E, Bissig B, Löckinger J, Fuchs P, Carron R, Weiss T P, Perrenoud J, Stutterheim S, Buecheler S and Tiwari A N 2017 Progress in thin film CIGS photovoltaics – Research and development, manufacturing, and applications *Prog. Photovolt. Res. Appl.* **25** 645-67
[6] Ono L K, Park N-G, Zhu K, Huang W and Qi Y B 2017 Perovskite Solar Cells—Towards Commercialization *ACS Energy Lett.* **2** 1749-51
[7] Qiu L, Ono L K and Qi Y B 2017 Advances and challenges to the commercialization of organic–inorganic halide perovskite solar cell technology *Mater. Today Energy* DOI:10.1016/j.mtener.2017.09.008
[8] Raga S R, Jiang Y, Ono L K and Qi Y B 2017 Application of Methylamine Gas in Fabricating Organic-Inorganic Hybrid Perovskite Solar Cells *Energy Technol.* **5** 1750-61
[9] Ono L K, Leyden M R, Wang S and Qi Y B 2016 Organometal Halide Perovskite Thin Films and Solar Cells by Vapor Deposition *J. Mater. Chem. A* **4** 6693-713
[10] National Renewable Energy Laboratory (NREL). Research Cell Efficiency Records. http://www.nrel.gov/ncpv/images/efficiency_chart.jpg (Last date accessed: December 25th, 2017)
[11] Green M A, Hishikawa Y, Dunlop E D, Levi D H, Hohl-Ebinger J and Ho-Baillie A W Y 2018 Solar cell efficiency tables (version 51) *Prog. Photovolt. Res. Appl.* **26** 3-12
[12] Kojima A, Teshima K, Shirai Y and Miyasaka T 2009 Organometal Halide Perovskites as Visible-Light Sensitizers for Photovoltaic Cells *J. Am. Chem. Soc.* **131** 6050-1
[13] Kim H S, Lee C R, Im J H, Lee K B, Moehl T, Marchioro A, Moon S J, Humphry-Baker R, Yum J H, Moser J E, Grätzel M and Park N G 2012 Lead Iodide Perovskite Sensitized All-Solid-State Submicron Thin Film Mesoscopic Solar Cell with Efficiency Exceeding 9% *Sci. Rep.* **2** 591
[14] Hawash Z, Ono L K and Qi Y B 2017 Recent Advances in Spiro-MeOTAD Hole Transport Material and Its Applications in Organic-inorganic Halide Perovskite Solar Cells *Adv. Mater. Interfaces* **4** 1700623
[15] Correa-Baena J-P, Saliba M, Buonassisi T, Grätzel M, Abate A, Tress W and Hagfeldt A 2017 Promises and challenges of perovskite solar cells *Science* **358** 739-44
[16] Shockley W and Queisser H J 1961 Detailed Balance Limit of Efficiency of P-N Junction Solar Cells *J. Appl. Phys.* **32** 510-9
[17] Sha W E I, Ren X, Chen L and Choy W C H 2015 The efficiency limit of $CH_3NH_3PbI_3$ perovskite solar cells *Appl. Phys. Lett.* **106** 221104
[18] Ono L K, Juárez-Pérez E J and Qi Y B 2017 Progress on Novel Perovskite Materials and Solar Cells with Mixed Cations and Halide Anions *ACS Appl. Mater. Interfaces* DOI: 10.1021/acsami.7b06001
[19] Polman A, Knight M, Garnett E C, Ehrler B and Sinke W C 2016 Photovoltaic materials: Present efficiencies and future challenges *Science* **352** aad4424
[20] Yoshikawa K, Kawasaki H, Yoshida W, Irie T, Konishi K, Nakano K, Uto T, Adachi D, Kanematsu M, Uzu H and Yamamoto K 2017 Silicon heterojunction solar cell with interdigitated back contacts for a photoconversion efficiency over 26% *Nat. Energy* **2** 17032
[21] Ribeyron P J 2017 Crystalline Silicon Solar Cells - Better Than Ever *Nat. Energy* **2** 17067

[22] Jeon N J, Noh J H, Yang W S, Kim Y C, Ryu S, Seo J and Seok S I 2015 Compositional Engineering of Perovskite Materials for High-Performance Solar Cells *Nature* **517** 476-80
[23] Adinolfi V, Peng W, Walters G, Bakr O M and Sargent E H 2017 The Electrical and Optical Properties of Organometal Halide Perovskites Relevant to Optoelectronic Performance *Adv. Mater.* **29** 1700764
[24] Brenner T M, Egger D A, Kronik L, Hodes G and Cahen D 2016 Hybrid Organic—Inorganic Perovskites: Low-Cost Semiconductors with Intriguing Charge-Transport Properties *Nat. Rev. Mater.* **1** 15007
[25] Huang J, Yuan Y, Shao Y and Yan Y 2017 Understanding the physical properties of hybrid perovskites for photovoltaic applications *Nat. Rev. Mater.* **2** 17042
[26] Berry J, Buonassisi T, Egger D A, Hodes G, Kronik L, Loo Y-L, Lubomirsky I, Marder S R, Mastai Y, Miller J S, Mitzi D B, Paz Y, Rappe A M, Riess I, Rybtchinski B, Stafsudd O, Stevanovic V, Toney M F, Zitoun D, Kahn A, Ginley D and Cahen D 2015 Hybrid Organic–Inorganic Perovskites (HOIPs): Opportunities and Challenges *Adv. Mater.* **27** 5102-12
[27] Brivio F, Butler K T, Walsh A and van Schilfgaarde M 2014 Relativistic Quasiparticle Self-Consistent Electronic Structure of Hybrid Halide Perovskite Photovoltaic Absorbers *Phys. Rev. B* **89** 155204
[28] Brandt R E, Stevanović V, Ginley D S and Buonassisi T 2015 Identifying defect-tolerant semiconductors with high minority-carrier lifetimes: beyond hybrid lead halide perovskites *MRS Commun.* **5** 265-75
[29] deQuilettes D W, Vorpahl S M, Stranks S D, Nagaoka H, Eperon G E, Ziffer M E, Snaith H J and Ginger D S 2015 Impact Of Microstructure On Local Carrier Lifetime In Perovskite Solar Cells *Science* **348** 683-6
[30] deQuilettes D W, Zhang W, Burlakov V M, Graham D J, Leijtens T, Osherov A, Bulović V, Snaith H J, Ginger D S and Stranks S D 2016 Photo-induced halide redistribution in organic–inorganic perovskite films *Nat. Commun.* **7** 11683
[31] De Wolf S, Holovsky J, Moon S J, Loper P, Niesen B, Ledinsky M, Haug F J, Yum J H and Ballif C 2014 Organometallic Halide Perovskites: Sharp Optical Absorption Edge and Its Relation to Photovoltaic Performance *J. Phys. Chem. Lett.* **5** 1035-9
[32] Sadhanala A, Deschler F, Thomas T H, Dutton S E, Goedel K C, Hanusch F C, Lai M L, Steiner U, Bein T, Docampo P, Cahen D and Friend R H 2014 Preparation of Single-Phase Films of $CH_3NH_3Pb(I_{1-x}Br_x)_3$ with Sharp Optical Band Edges *J. Phys. Chem. Lett.* **5** 2501-5
[33] Fedeli P, Gazza F, Calestani D, Ferro P, Besagni T, Zappettini A, Calestani G, Marchi E, Ceroni P and Mosca R 2015 Influence of the Synthetic Procedures on the Structural and Optical Properties of Mixed-Halide (Br,I) Perovskite Films *J. Phys. Chem. C* **119** 21304-13
[34] Rehman W, Milot R L, Eperon G E, Wehrenfennig C, Boland J L, Snaith H J, Johnston M B and Herz L M 2015 Charge-Carrier Dynamics and Mobilities in Formamidinium Lead Mixed-Halide Perovskites *Adv. Mater.* **27** 7938-44
[35] Hoke E T, Slotcavage D J, Dohner E R, Bowring A R, Karunadasa H I and McGehee M D 2015 Reversible Photo-Induced Trap Formation in Mixed-Halide Hybrid Perovskites for Photovoltaics *Chem. Sci.* **6** 613-7
[36] Yang X, Yan X, Wang W, Zhu X, Li H, Ma W and Sheng C 2016 Light Induced Metastable Modification of Optical Properties in $CH_3NH_3PbI_{3-x}Br_x$ Perovskite Films: Two-Step Mechanism *Org. Electron.* **34** 79-83

[37] Bischak C G, Hetherington C L, Wu H, Aloni S, Ogletree D F, Limmer D T and Ginsberg N S 2017 Origin of Reversible Photoinduced Phase Separation in Hybrid Perovskites *Nano Lett.* **17** 1028-33
[38] Brivio F, Caetano C and Walsh A 2016 Thermodynamic Origin of Photoinstability in the $CH_3NH_3Pb(I_{1-x}Br_x)_3$ Hybrid Halide Perovskite Alloy *J. Phys. Chem. Lett.* **7** 1083-7
[39] Yoon S J, Draguta S, Manser J S, Sharia O, Schneider W F, Kuno M and Kamat P V 2016 Tracking Iodide and Bromide Ion Segregation in Mixed Halide Lead Perovskites during Photoirradiation *ACS Energy Lett.* **1** 290-6
[40] Slotcavage D J, Karunadasa H I and McGehee M D 2016 Light-Induced Phase Segregation in Halide-Perovskite Absorbers *ACS Energy Lett.* **1** 1199-205
[41] Barker A J, Sadhanala A, Deschler F, Gandini M, Senanayak S P, Pearce P M, Mosconi E, Pearson A J, Wu Y, Srimath Kandada A R, Leijtens T, De Angelis F, Dutton S E, Petrozza A and Friend R H 2017 Defect-Assisted Photoinduced Halide Segregation in Mixed-Halide Perovskite Thin Films *ACS Energy Lett.* **2** 1416-24
[42] Draguta S, Sharia O, Yoon S J, Brennan M C, Morozov Y V, Manser J M, Kamat P V, Schneider W F and Kuno M 2017 Rationalizing the light-induced phase separation of mixed halide organic–inorganic perovskites *Nat. Commun.* **8** 200
[43] Unger E L, Kegelmann L, Suchan K, Sörell D, Korte L and Albrecht S 2017 Roadmap and Roadblocks for the Band Gap Tunability of Metal Halide Perovskites *J. Mater. Chem. A* **5** 11401-9
[44] Hu M, Bi C, Yuan Y, Bai Y and Huang J 2016 Stabilized Wide Bandgap $MAPbBr_xI_{3-x}$ Perovskite by Enhanced Grain Size and Improved Crystallinity *Adv. Sci.* **3** 1500301
[45] Beal R E, Slotcavage D J, Leijtens T, Bowring A R, Belisle R A, Nguyen W H, Burkhard G F, Hoke E T and McGehee M D 2016 Cesium Lead Halide Perovskites with Improved Stability for Tandem Solar Cells *J. Phys. Chem. Lett.* **7** 746-51
[46] McMeekin D P, Sadoughi G, Rehman W, Eperon G E, Saliba M, Hörantner M T, Haghighirad A, Sakai N, Korte L, Rech B, Johnston M B, Herz L M and Snaith H J 2016 A Mixed-Cation Lead Mixed-Halide Perovskite Absorber for Tandem Solar Cells *Science* **351** 151-5
[47] Saliba M, Matsui T, Domanski K, Seo J Y, Ummadisingu A, Zakeeruddin S M, Correa-Baena J P, Tress W R, Abate A, Hagfeldt A and Gratzel M 2016 Incorporation of Rubidium Cations Into Perovskite Solar Cells Improves Photovoltaic Performance *Science* **354** 206-9
[48] Yang Z, Rajagopal A, Jo S B, Chueh C-C, Williams S, Huang C-C, Katahara J K, Hillhouse H W and Jen A K Y 2016 Stabilized Wide Bandgap Perovskite Solar Cells by Tin Substitution *Nano Lett.* **16** 7739-47
[49] Duong T, Wu Y, Shen H, Peng J, Fu X, Jacobs D, Wang E-C, Kho T C, Fong K C, Stocks M, Franklin E, Blakers A, Zin N, McIntosh K, Li W, Cheng Y-B, White T P, Weber K and Catchpole K 2017 Rubidium Multication Perovskite with Optimized Bandgap for Perovskite-Silicon Tandem with over 26% Efficiency *Adv. Energy Mater.* **7** 1700228
[50] Akkerman Q A, D'Innocenzo V, Accornero S, Scarpellini A, Petrozza A, Prato M and Manna L 2015 Tuning the Optical Properties of Cesium Lead Halide Perovskite Nanocrystals by Anion Exchange Reactions *J. Am. Chem. Soc.* **137** 10276-81
[51] Samu G F, Janáky C and Kamat P V 2017 A Victim of Halide Ion Segregation. How Light Soaking Affects Solar Cell Performance of Mixed Halide Lead Perovskites *ACS Energy Lett.* **2** 1860-1
[52] Duong T, Mulmudi H K, Wu Y, Fu X, Shen H, Peng J, Wu N, Nguyen H T, Macdonald D, Lockrey M, White T P, Weber K and Catchpole K 2017 Light and Electrically

Induced Phase Segregation and Its Impact on the Stability of Quadruple Cation High Bandgap Perovskite Solar Cells *ACS Appl. Mater. Interfaces* **9** 26859-66

[53] Bakulin A A, Selig O, Bakker H J, Rezus Y L A, Müller C, Glaser T, Lovrincic R, Sun Z, Chen Z, Walsh A, Frost J M and Jansen T L C 2015 Real-Time Observation of Organic Cation Reorientation in Methylammonium Lead Iodide Perovskites *J. Phys. Chem. Lett.* **6** 3663-9

[54] Yuan Y and Huang J 2016 Ion Migration in Organometal Trihalide Perovskite and Its Impact on Photovoltaic Efficiency and Stability *Acc. Chem. Res.* **49** 286-93

[55] Nie W, Blancon J-C, Neukirch A J, Appavoo K, Tsai H, Chhowalla M, Alam M A, Sfeir M Y, Katan C, Even J, Tretiak S, Crochet J J, Gupta G and Mohite A D 2016 Light-activated photocurrent degradation and self-healing in perovskite solar cells *Nat. Commun.* **7** 11574

[56] Egger D A, Rappe A M and Kronik L 2016 Hybrid Organic–Inorganic Perovskites on the Move *Acc. Chem. Res.* **49** 573-81

[57] Whalley L D, Frost J M, Jung Y-K and Walsh A 2017 Perspective: Theory and simulation of hybrid halide perovskites *J. Chem. Phys.* **146** 220901

[58] Onoda-Yamamuro N, Matsuo T and Suga H 1990 Calorimetric and IR spectroscopic studies of phase transitions in methylammonium trihalogenoplumbates(II) *J. Phys. Chem. Solids* **51** 1383-95

[59] Leguy A M A, Frost J M, McMahon A P, Sakai V G, Kockelmann W, Law C, Li X, Foglia F, Walsh A, O/'Regan B C, Nelson J, Cabral J T and Barnes P R F 2015 The Dynamics of Methylammonium Ions in Hybrid Organic-Inorganic Perovskite Solar Cells *Nat. Commun.* **6** 7124

[60] Leguy A M A, Goni A R, Frost J M, Skelton J, Brivio F, Rodriguez-Martinez X, Weber O J, Pallipurath A, Alonso M I, Campoy-Quiles M, Weller M T, Nelson J, Walsh A and Barnes P R F 2016 Dynamic Disorder, Phonon Lifetimes, and the Assignment of Modes to the Vibrational Spectra of Methylammonium Lead Halide Perovskites *Phys. Chem. Chem. Phys.* **18** 27051-66

[61] Beecher A N, Semonin O E, Skelton J M, Frost J M, Terban M W, Zhai H, Alatas A, Owen J S, Walsh A and Billinge S J L 2016 Direct Observation of Dynamic Symmetry Breaking above Room Temperature in Methylammonium Lead Iodide Perovskite *ACS Energy Lett.* **1** 880-7

[62] Berdiyorov G R, El-Mellouhi F, Madjet M E, Alharbi F H and Rashkeev S N 2016 Electronic transport in organometallic perovskite $CH_3NH_3PbI_3$: The role of organic cation orientations *Appl. Phys. Lett.* **108** 053901

[63] Gong J, Yang M, Ma X, Schaller R D, Liu G, Kong L, Yang Y, Beard M C, Lesslie M, Dai Y, Huang B, Zhu K and Xu T 2016 Electron–Rotor Interaction in Organic–Inorganic Lead Iodide Perovskites Discovered by Isotope Effects *J. Phys. Chem. Lett.* **7** 2879-87

[64] Deretzis I, Di Mauro B N, Alberti A, Pellegrino G, Smecca E and La Magna A 2016 Spontaneous bidirectional ordering of $CH_3NH_3^+$ in lead iodide perovskites at room temperature: The origins of the tetragonal phase *Sci. Rep.* **6** 24443

[65] Carignano M A, Saeed Y, Aravindh S A, Roqan I S, Even J and Katan C 2016 A Close Examination of the Structure and Dynamics of $HC(NH_2)_2PbI_3$ by MD Simulations and Group Theory *Phys. Chem. Chem. Phys.* **18** 27109-18

[66] Frost J M and Walsh A 2016 What Is Moving in Hybrid Halide Perovskite Solar Cells? *Acc. Chem. Res.* **49** 528-35

[67] Saliba M, Correa-Baena J-P, Graetzel M, Hagfeldt A and Abate A 2017 Perovskite solar cells from the atomic to the film level *Angew. Chem. Int. Ed.* DOI: 10.1002/anie.201703226

[68] Wu X, Tan L Z, Shen X, Hu T, Miyata K, Trinh M T, Li R, Coffee R, Liu S, Egger D A, Makasyuk I, Zheng Q, Fry A, Robinson J S, Smith M D, Guzelturk B, Karunadasa H I, Wang X, Zhu X, Kronik L, Rappe A M and Lindenberg A M 2017 Light-induced picosecond rotational disordering of the inorganic sublattice in hybrid perovskites *Sci. Adv.* **3** e1602388

[69] Motta C, El-Mellouhi F, Kais S, Tabet N, Alharbi F and Sanvito S 2015 Revealing the Role of Organic Cations in Hybrid Halide Perovskite $CH_3NH_3PbI_3$ *Nat. Commun.* **6** 7026

[70] Frost J M, Butler K T, Brivio F, Hendon C H, van Schilfgaarde M and Walsh A 2014 Atomistic Origins of High-Performance in Hybrid Halide Perovskite Solar Cells *Nano Lett.* **14** 2584-90

[71] Ma J and Wang L-W 2015 Nanoscale Charge Localization Induced by Random Orientations of Organic Molecules in Hybrid Perovskite $CH_3NH_3PbI_3$ *Nano Lett.* **15** 248-53

[72] Mosconi E, Etienne T and De Angelis F 2017 Rashba Band Splitting in Organohalide Lead Perovskites: Bulk and Surface Effects **8** 2247-52

[73] Neukirch A J, Nie W, Blancon J-C, Appavoo K, Tsai H, Sfeir M Y, Katan C, Pedesseau L, Even J, Crochet J J, Gupta G, Mohite A D and Tretiak S 2016 Polaron Stabilization by Cooperative Lattice Distortion and Cation Rotations in Hybrid Perovskite Materials *Nano Lett.* **16** 3809-16

[74] Rashkeev S N, El-Mellouhi F, Kais S and Alharbi F H 2015 Domain Walls Conductivity in Hybrid Organometallic Perovskites and Their Essential Role in CH3NH3PbI3 Solar Cell High Performance *Sci. Rep.* **5** 11467

[75] Murali B, Yengel E, Yang C, Peng W, Alarousu E, Bakr O M and Mohammed O F 2017 The Surface of Hybrid Perovskite Crystals: A Boon or Bane *ACS Energy Lett.* **2** 846-56

[76] Haruyama J, Sodeyama K, Han L and Tateyama Y 2016 Surface Properties of $CH_3NH_3PbI_3$ for Perovskite Solar Cells *Acc. Chem. Res.* **49** 554-61

[77] Ono L K and Qi Y B 2016 Surface and Interface Aspects of Organometal Halide Perovskite Materials and Solar Cells *J. Phys. Chem. Lett.* **7** 4764-94

[78] Ohmann R, Ono L K, Kim H-S, Lin H, Lee M V, Li Y, Park N-G and Qi Y B 2015 Real-Space Imaging of the Atomic Structure of Organic–Inorganic Perovskite *J. Am. Chem. Soc.* **137** 16049-54

[79] Hawash Z, Raga S R, Son D-Y, Ono L K, Park N-G and Qi Y 2017 Interfacial Modification of Perovskite Solar Cells Using an Ultrathin MAI Layer Leads to Enhanced Energy Level Alignment, Efficiencies, and Reproducibility *J. Phys. Chem. Lett.* **8** 3947-53

[80] Xing J, Wang Q, Dong Q, Yuan Y, Fang Y and Huang J 2016 Ultrafast Ion Migration in Hybrid Perovskite Polycrystalline Thin Films under Light and Suppression in Single Crystals *Phys. Chem. Chem. Phys.* **18** 30484-90

[81] Azpiroz J M, Mosconi E, Bisquert J and De Angelis F 2015 Defect Migration in Methylammonium Lead Iodide and Its Role in Perovskite Solar Cell Operation *Energy Environ. Sci.* **8** 2118-27

[82] Domanski K, Roose B, Matsui T, Saliba M, Turren-Cruz S H, Correa-Baena J P, Carmona C R, Richardson G, Foster J M, De Angelis F, Ball J M, Petrozza A, Mine N, Nazeeruddin M K, Tress W, Gratzel M, Steiner U, Hagfeldt A and Abate A 2017 Migration of Cations Induces Reversible Performance Losses Over Day/Night Cycling in Perovskite Solar Cells *Energy Environ. Sci.* **10** 604-13

[83] Momblona C, Gil-Escrig L, Bandiello E, Hutter E M, Sessolo M, Lederer K, Blochwitz-Nimoth J and Bolink H J 2016 Efficient Vacuum Deposited p-i-n and n-i-p Perovskite

Solar Cells Employing Doped Charge Transport Layers *Energy Environ. Sci.* **9** 3456-63
[84] Laban W A and Etgar L 2013 Depleted Hole Conductor-Free Lead Halide Iodide Heterojunction Solar Cells *Energy Environ. Sci.* **6** 3249-53
[85] Etgar L, Gao P, Xue Z, Peng Q, Chandiran A K, Liu B, Nazeeruddin M K and Grätzel M 2012 Mesoscopic $CH_3NH_3PbI_3/TiO_2$ Heterojunction Solar Cells *J. Am. Chem. Soc.* **134** 17396-9
[86] Chen H and Yang S 2017 Carbon-Based Perovskite Solar Cells without Hole Transport Materials: The Front Runner to the Market? *Adv. Energy Mater.* **7** 1603994
[87] Mei A, Li X, Liu L, Ku Z, Liu T, Rong Y, Xu M, Hu M, Chen J, Yang Y, Grätzel M and Han H 2014 A Hole-Conductor–Free, Fully Printable Mesoscopic Perovskite Solar Cell with High Stability *Science* **345** 295-8
[88] Correa-Baena J P, Tress W, Domanski K, Anaraki E H, Turren-Cruz S H, Roose B, Boix P P, Gratzel M, Saliba M, Abate A and Hagfeldt A 2017 Identifying and suppressing interfacial recombination to achieve high open-circuit voltage in perovskite solar cells *Energy Environ. Sci.* **10** 1207-12
[89] Tan H, Jain A, Voznyy O, Lan X, García de Arquer F P, Fan J Z, Quintero-Bermudez R, Yuan M, Zhang B, Zhao Y, Fan F, Li P, Quan L N, Zhao Y, Lu Z-H, Yang Z, Hoogland S and Sargent E H 2017 Efficient and Stable Solution-Processed Planar Perovskite Solar Cells via Contact Passivation *Science* **355** 722-6
[90] Fang H-H, Adjokatse S, Wei H, Yang J, Blake G R, Huang J, Even J and Loi M A 2016 Ultrahigh Sensitivity of Methylammonium Lead Tribromide Perovskite Single Crystals to Environmental Gases *Sci. Adv.* **2** e1600534
[91] Elbaz G A, Straus D B, Semonin O E, Hull T D, Paley D W, Kim P, Owen J S, Kagan C R and Roy X 2017 Unbalanced Hole and Electron Diffusion in Lead Bromide Perovskites *Nano Lett.* **17** 1727-32
[92] Bergmann V W, Weber S A L, Javier Ramos F, Nazeeruddin M K, Grätzel M, Li D, Domanski A L, Lieberwirth I, Ahmad S and Berger R 2014 Real-Space Observation of Unbalanced Charge Distribution Inside a Perovskite-Sensitized Solar Cell *Nat. Commun.* **5** 5001
[93] Bergmann V W, Guo Y, Tanaka H, Hermes I M, Li D, Klasen A, Bretschneider S A, Nakamura E, Berger R and Weber S A L 2016 Local Time-Dependent Charging in a Perovskite Solar Cell *ACS Appl. Mater. Interfaces* **8** 19402-9
[94] Jiang C-S, Yang M, Zhou Y, To B, Nanayakkara S U, Luther J M, Zhou W, Berry J J, van de Lagemaat J, Padture N P, Zhu K and Al-Jassim M M 2015 Carrier Separation and Transport in Perovskite Solar Cells Studied by Nanometre-Scale Profiling of Electrical Potential *Nat. Commun.* **6** 8397
[95] Guerrero A, Juarez-Perez E J, Bisquert J, Mora-Sero I and Garcia-Belmonte G 2014 Electrical Field Profile and Doping in Planar Lead Halide Perovskite Solar Cells *Appl. Phys. Lett.* **105** 133902
[96] Chen Q, Mao L, Li Y, Kong T, Wu N, Ma C, Bai S, Jin Y, Wu D, Lu W, Wang B and Chen L 2015 Quantitative Operando Visualization of the Energy Band Depth Profile in Solar Cells *Nat. Commun.* **6** 7745
[97] Wang C, Xiao C, Yu Y, Zhao D, Awni R A, Grice C R, Ghimire K, Constantinou I, Liao W, Cimaroli A J, Liu P, Chen J, Podraza N J, Jiang C-S, Al-Jassim M M, Zhao X and Yan Y 2017 Understanding and Eliminating Hysteresis for Highly Efficient Planar Perovskite Solar Cells *Adv. Energy Mater.* **7** 1700414
[98] Ou Q-D, Li C, Wang Q-K, Li Y-Q and Tang J-X 2017 Recent Advances in Energetics of Metal Halide Perovskite Interfaces *Adv. Mater. Interfaces* **4** 1600694

[99] Wang Q K, Wang R B, Shen P F, Li C, Li Y Q, Liu L J, Duhm S and Tang J X 2015 Energy Level Offsets at Lead Halide Perovskite/Organic Hybrid Interfaces and Their Impacts on Charge Separation *Adv. Mater. Interfaces* **2** 1400528
[100] Schulz P, Edri E, Kirmayer S, Hodes G, Cahen D and Kahn A 2014 Interface Energetics in Organo-Metal Halide Perovskite-Based Photovoltaic Cells *Energy Environ. Sci.* **7** 1377-81
[101] Schulz P, Whittaker-Brooks L L, MacLeod B A, Olson D C, Loo Y-L and Kahn A 2015 Electronic Level Alignment in Inverted Organometal Perovskite Solar Cells *Adv. Mater. Interfaces* **2** 1400532
[102] Schulz P, Tiepelt J O, Christians J A, Levine I, Edri E, Sanehira E M, Hodes G, Cahen D and Kahn A 2016 High-Work-Function Molybdenum Oxide Hole Extraction Contacts in Hybrid Organic–Inorganic Perovskite Solar Cells *ACS Appl. Mater. Interfaces* **8** 31491-9
[103] Schulz P, Dowgiallo A-M, Yang M, Zhu K, Blackburn J L and Berry J J 2016 Charge Transfer Dynamics between Carbon Nanotubes and Hybrid Organic Metal Halide Perovskite Films *J. Phys. Chem. Lett.* **7** 418-25
[104] Endres J, Egger D A, Kulbak M, Kerner R A, Zhao L, Silver S H, Hodes G, Rand B P, Cahen D, Kronik L and Kahn A 2016 Valence and Conduction Band Densities of States of Metal Halide Perovskites: A Combined Experimental–Theoretical Study *J. Phys. Chem. Lett.* **7** 2722-9
[105] Endres J, Kulbak M, Zhao L, Rand B P, Cahen D, Hodes G and Kahn A 2017 Electronic structure of the $CsPbBr_3$/polytriarylamine (PTAA) system *J. Appl. Phys.* **121** 035304
[106] Li C, Wei J, Sato M, Koike H, Xie Z-Z, Li Y-Q, Kanai K, Kera S, Ueno N and Tang J-X 2016 Halide-Substituted Electronic Properties of Organometal Halide Perovskite Films: Direct and Inverse Photoemission Studies *ACS Appl. Mater. Interfaces* **8** 11526-31
[107] Liu P, Liu X L, Lyu L, Xie H P, Zhang H, Niu D M, Huang H, Bi C, Xiao Z G, Huang J S and Gao Y L 2015 Interfacial Electronic Structure at the $CH_3NH_3PbI_3/MoO_x$ Interface *Appl. Phys. Lett.* **106** 193903
[108] Liu X L, Wang C G, Lyu L, Wang C C, Xiao Z G, Bi C, Huang J S and Gao Y L 2015 Electronic Structures at the Interface between Au and $CH_3NH_3PbI_3$ *Phys. Chem. Chem. Phys.* **17** 896-902
[109] Chen S, Goh T W, Sabba D, Chua J, Mathews N, Huan C H A and Sum T C 2014 Energy Level Alignment at the Methylammonium Lead Iodide/Copper Phthalocyanine Interface *APL Mater.* **2** 081512
[110] Ji G, Zhao B, Song F, Zheng G, Zhang X, Shen K, Yang Y, Chen S and Gao X 2017 The energy level alignment at the $CH_3NH_3PbI_3$/pentacene interface *Appl. Surf. Sci.* **393** 417-21
[111] Wolff C M, Zu F, Paulke A, Toro L P, Koch N and Neher D 2017 Reduced Interface-Mediated Recombination for High Open-Circuit Voltages in $CH_3NH_3PbI_3$ Solar Cells *Adv. Mater.* **29** 1700159
[112] Miller E M, Zhao Y X, Mercado C C, Saha S K, Luther J M, Zhu K, Stevanovic V, Perkins C L and van de Lagemaat J 2014 Substrate-Controlled Band Positions in $CH_3NH_3Pbl_3$ Perovskite Films *Phys. Chem. Chem. Phys.* **16** 22122-30
[113] Zou Y, Meng Q, Mao H and Zhu D 2017 Substrate Effect on the Interfacial Electronic Structure of Thermally-Evaporated $CH_3NH_3PbI_3$ Perovskite Layer *Org. Electron.* **41** 307-14
[114] Emara J, Schnier T, Pourdavoud N, Riedl T, Meerholz K and Olthof S 2016 Impact of Film Stoichiometry on the Ionization Energy and Electronic Structure of $CH_3NH_3PbI_3$ Perovskites *Adv. Mater.* **28** 553-9

[115] Kahn A 2016 Fermi level, work function and vacuum level *Mater. Horiz.* **3** 7-10
[116] Olthof S 2016 Research Update: The Electronic Structure of Hybrid Perovskite Layers and their Energetic Alignment in Devices *APL Mater.* **4** 091502
[117] Olthof S and Meerholz K 2017 Substrate-Dependent Electronic Structure and Film Formation of $MAPbI_3$ Perovskites *Sci. Rep.* **7** 40267
[118] Zhang Y, Wu Z, Li P, Ono L K, Qi Y, Zhou J, Shen H, Surya C and Zheng Z 2017 Fully Solution-Processed TCO-Free Semitransparent Perovskite Solar Cells for Tandem and Flexible Applications *Adv. Energy Mater.* **7** 1701569
[119] Lim K-G, Ahn S, Kim Y-H, Qi Y B and Lee T-W 2016 Universal Energy Level Tailoring of Self-Organized Hole Extraction Layers in Organic Solar Cells and Organic-Inorganic Hybrid Perovskite Solar Cells *Energy Environ. Sci.* **9** 932-9
[120] Wu X, Trinh M T, Niesner D, Zhu H, Norman Z, Owen J S, Yaffe O, Kudisch B J and Zhu X Y 2015 Trap States in Lead Iodide Perovskites *J. Am. Chem. Soc.* **137** 2089-96
[121] Kollár M, Ćirić L, Dil J H, Weber A, Muff S, Ronnow H M, Náfrádi B, Monnier B P, Luterbacher J S, Forró L and Horváth E 2017 Clean, cleaved surfaces of the photovoltaic perovskite *Sci. Rep.* **7** 695
[122] Lee M-I, Barragán A, Nair M N, Jacques V L R, Le Bolloc'h D, Fertey P, Jemli K, Lédée F, Trippé-Allard G, Deleporte E, Taleb-Ibrahimi A and Tejeda A 2017 First determination of the valence band dispersion of $CH_3NH_3PbI_3$ hybrid organic–inorganic perovskite *J. Phys. D: Appl. Phys.* **50** 26LT02
[123] Wang C, Ecker B R, Wei H, Huang J, Meng J-Q and Gao Y 2017 Valence band dispersion measurements of perovskite single crystals using angle-resolved photoemission spectroscopy *Phys. Chem. Chem. Phys.* **19** 5361-5
[124] Heo S, Seo G, Lee Y, Lee D, Seol M, Lee J, Park J B, Kim K, Yun D J, Kim Y S, Shin J K, Ahn T K and Nazeeruddin M K 2017 Deep Level Trapped Defect Analysis in $CH_3NH_3PbI_3$ Perovskite Solar Cells by Deep Level Transient Spectroscopy *Energy Environ. Sci.* **10** 1128-33
[125] Adinolfi V, Yuan M, Comin R, Thibau E S, Shi D, Saidaminov M I, Kanjanaboos P, Kopilovic D, Hoogland S, Lu Z-H, Bakr O M and Sargent E H 2016 The In-Gap Electronic State Spectrum of Methylammonium Lead Iodide Single-Crystal Perovskites *Adv. Mater.* **28** 3406-10
[126] Dualeh A, Moehl T, Tétreault N, Teuscher J, Gao P, Nazeeruddin M K and Grätzel M 2014 Impedance Spectroscopic Analysis of Lead Iodide Perovskite-Sensitized Solid-State Solar Cells *ACS Nano* **8** 362-73
[127] Nemnes G A, Besleaga C, Stancu V, Dogaru D E, Leonat L N, Pintilie L, Torfason K, Ilkov M, Manolescu A and Pintilie I 2017 Normal and Inverted Hysteresis in Perovskite Solar Cells *J. Phys. Chem. C* **121** 11207-14
[128] Hu J, Gottesman R, Gouda L, Kama A, Priel M, Tirosh S, Bisquert J and Zaban A 2017 Photovoltage Behavior in Perovskite Solar Cells under Light-Soaking Showing Photoinduced Interfacial Changes *ACS Energy Lett.* **2** 950-6
[129] Raga S R and Qi Y 2016 The Effect of Impurities on the Impedance Spectroscopy Response of $CH_3NH_3PbI_3$ Perovskite Solar Cells *J. Phys. Chem. C* **120** 28519-26
[130] Zarazua I, Han G, Boix P P, Mhaisalkar S, Fabregat-Santiago F, Mora-Seró I, Bisquert J and Garcia-Belmonte G 2016 Surface Recombination and Collection Efficiency in Perovskite Solar Cells from Impedance Analysis *J. Phys. Chem. Lett.* **7** 5105-13
[131] Ghahremanirad E, Bou A, Olyaee S and Bisquert J 2017 Inductive Loop in the Impedance Response of Perovskite Solar Cells Explained by Surface Polarization Model *J. Phys. Chem. Lett.* **8** 1402-6
[132] Fakharuddin A, Schmidt-Mende L, Garcia-Belmonte G, Jose R and Mora-Sero I 2017 Interfaces in Perovskite Solar Cells *Adv. Energy Mater.* **7** 1700623

[133] Pockett A, Eperon G E, Sakai N, Snaith H J, Peter L M and Cameron P J 2017 Microseconds, Milliseconds and Seconds: Deconvoluting The Dynamic Behaviour of Planar Perovskite Solar Cells *Phys. Chem. Chem. Phys.* **19** 5959-70
[134] Li C, Guerrero A, Zhong Y, Gräser A, Luna C A M, Köhler J, Bisquert J, Hildner R and Huettner S 2017 Real-Time Observation of Iodide Ion Migration in Methylammonium Lead Halide Perovskites *Small* **13** 1701711
[135] Correa-Baena J-P, Turren-Cruz S-H, Tress W, Hagfeldt A, Aranda C, Shooshtari L, Bisquert J and Guerrero A 2017 Changes from Bulk to Surface Recombination Mechanisms between Pristine and Cycled Perovskite Solar Cells *ACS Energy Lett.* **2** 681-8
[136] Ravishankar S, Almora O, Echeverría-Arrondo C, Ghahremanirad E, Aranda C, Guerrero A, Fabregat-Santiago F, Zaban A, Garcia-Belmonte G and Bisquert J 2017 Surface Polarization Model for the Dynamic Hysteresis of Perovskite Solar Cells *J. Phys. Chem. Lett.* **8** 915-21
[137] Vicente N and Garcia-Belmonte G 2017 Methylammonium Lead Bromide Perovskite Battery Anodes Reversibly Host High Li-Ion Concentrations *J. Phys. Chem. Lett.* **8** 1371-4
[138] Dawson J A, Naylor A J, Eames C, Roberts M, Zhang W, Snaith H J, Bruce P G and Islam M S 2017 Mechanisms of Lithium Intercalation and Conversion Processes in Organic–Inorganic Halide Perovskites *ACS Energy Lett.* **2** 1818-24
[139] Tathavadekar M, Krishnamurthy S, Banerjee A, Nagane S, Gawli Y, Suryawanshi A, Bhat S, Puthusseri D, Mohite A D and Ogale S 2017 Low-dimensional hybrid perovskites as high performance anodes for alkali-ion batteries *J. Mater. Chem. A* **5** 18634-42
[140] Belisle R A, Nguyen W H, Bowring A R, Calado P, Li X, Irvine S J C, McGehee M D, Barnes P R F and O'Regan B C 2017 Interpretation of Inverted Photocurrent Transients in Organic Lead Halide Perovskite Solar Cells: Proof of the Field Screening by Mobile Ions and Determination of the Space Charge Layer Widths *Energy Environ. Sci.* **10** 192-204
[141] Rong Y, Hu Y, Ravishankar S, Liu H, Hou X, Sheng Y, Mei A, Wang Q, Li D, Xu M, Bisquert J and Han H 2017 Tunable hysteresis effect for perovskite solar cells *Energy Environ. Sci.* DOI: 10.1039/C7EE02048A
[142] Jacobs D A, Wu Y, Shen H, Barugkin C, Beck F J, White T P, Weber K and Catchpole K R 2017 Hysteresis phenomena in perovskite solar cells: the many and varied effects of ionic accumulation *Phys. Chem. Chem. Phys.* **19** 3094-103
[143] Sherkar T S, Momblona C, Gil-Escrig L, Ávila J, Sessolo M, Bolink H J and Koster L J A 2017 Recombination in Perovskite Solar Cells: Significance of Grain Boundaries, Interface Traps, and Defect Ions *ACS Energy Lett.* **2** 1214-22
[144] Ono L K, Raga S R, Wang S, Kato Y and Qi Y B 2015 Temperature-Dependent Hysteresis Effects in Perovskite-Based Solar Cells *J. Mater. Chem. A* **3** 9074-80
[145] Gottesman R, Lopez-Varo P, Gouda L, Jimenez-Tejada Juan A, Hu J, Tirosh S, Zaban A and Bisquert J 2016 Dynamic Phenomena at Perovskite/Electron-Selective Contact Interface as Interpreted from Photovoltage Decays *Chem.* **1** 776-89
[146] Garrett J L, Tennyson E M, Hu M, Huang J, Munday J N and Leite M S 2017 Real-Time Nanoscale Open-Circuit Voltage Dynamics of Perovskite Solar Cells *Nano Lett.* DOI: 10.1021/acs.nanolett.7b00289
[147] Gottesman R, Haltzi E, Gouda L, Tirosh S, Bouhadana Y, Zaban A, Mosconi E and De Angelis F 2014 Extremely Slow Photoconductivity Response of CH3NH3PbI3 Perovskites Suggesting Structural Changes under Working Conditions *J. Phys. Chem. Lett.* **5** 2662-9

[148] Levine I, Nayak P K, Wang J T-W, Sakai N, Van Reenen S, Brenner T M, Mukhopadhyay S, Snaith H J, Hodes G and Cahen D 2016 Interface-Dependent Ion Migration/Accumulation Controls Hysteresis in $MAPbI_3$ Solar Cells *J. Phys. Chem. C* **120** 16399-411
[149] Snaith H J, Abate A, Ball J M, Eperon G E, Leijtens T, Noel N K, Stranks S D, Wang J T-W, Wojciechowski K and Zhang W 2014 Anomalous Hysteresis in Perovskite Solar Cells *J. Phys. Chem. Lett.* **5** 1511-5
[150] van Reenen S, Kemerink M and Snaith H J 2015 Modeling Anomalous Hysteresis in Perovskite Solar Cells *J. Phys. Chem. Lett.* **6** 3808-14
[151] Tress W, Correa Baena J P, Saliba M, Abate A and Graetzel M 2016 Inverted Current–Voltage Hysteresis in Mixed Perovskite Solar Cells: Polarization, Energy Barriers, and Defect Recombination *Adv. Energy Mater.* **6** 1600396
[152] Shen H, Jacobs D A, Wu Y, Duong T, Peng J, Wen X, Fu X, Karuturi S K, White T P, Weber K and Catchpole K R 2017 Inverted Hysteresis in $CH_3NH_3PbI_3$ Solar Cells: Role of Stoichiometry and Band Alignment *J. Phys. Chem. Lett.* **8** 2672-80
[153] Calado P, Telford A M, Bryant D, Li X, Nelson J, O'Regan B C and Barnes P R F 2016 Evidence for ion migration in hybrid perovskite solar cells with minimal hysteresis *Nat. Commun.* **7** 13831
[154] Shao Y, Xiao Z, Bi C, Yuan Y and Huang J 2014 Origin and Elimination of Photocurrent Hysteresis by Fullerene Passivation in $CH_3NH_3PbI_3$ Planar Heterojunction Solar Cells *Nat. Commun.* **5** 5784
[155] Xu J, Buin A, Ip A H, Li W, Voznyy O, Comin R, Yuan M, Jeon S, Ning Z, McDowell J J, Kanjanaboos P, Sun J-P, Lan X, Quan L N, Kim D H, Hill I G, Maksymovych P and Sargent E H 2015 Perovskite-Fullerene Hybrid Materials Suppress Hysteresis in Planar Diodes *Nat. Commun.* **6** 7081
[156] Song D H, Jang M H, Lee M H, Heo J H, Park J K, Sung S-J, Kim D-H, Hong K-H and Im S H 2016 A discussion on the origin and solutions of hysteresis in perovskite hybrid solar cells *J. Phys. D: Appl. Phys.* **49** 473001
[157] Heo J H, Han H J, Kim D, Ahn T K and Im S H 2015 Hysteresis-Less Inverted $CH_3NH_3PbI_3$ Planar Perovskite Hybrid Solar Cells with 18.1% Power Conversion Efficiency *Energy Environ. Sci.* **8** 1602-8
[158] Li Z, Xiao C, Yang Y, Harvey S P, Kim D H, Christians J A, Yang M, Schulz P, Nanayakkara S U, Jiang C-S, Luther J M, Berry J J, Beard M C, Al-Jassim M M and Zhu K 2017 Extrinsic ion migration in perovskite solar cells *Energy Environ. Sci.* **10** 1234-42
[159] Pockett A and Carnie M J 2017 Ionic influences on recombination in perovskite solar cells *ACS Energy Lett.* **2** 1683-9
[160] Lopez-Varo P, Jiménez-Tejada J A, García-Rosell M, Anta J A, Ravishankar S, Bou A and Bisquert J 2017 Effects of Ion Distributions on Charge Collection in Perovskite Solar Cells *ACS Energy Lett.* **2** 1450-3
[161] Li C, Guerrero A, Zhong Y and Huettner S 2017 Origins and mechanisms of hysteresis in organometal halide perovskites *J. Phys. Condens. Matter* **29** 193001
[162] Berry J J, van de Lagemaat J, Al-Jassim M M, Kurtz S, Yan Y and Zhu K 2017 Perovskite Photovoltaics: The Path to a Printable Terawatt-Scale Technology *ACS Energy Lett.* **2** 2540-4
[163] Leyden M R, Jiang Y and Qi Y B 2016 Chemical Vapor Deposition Grown Formamidinium Perovskite Solar Modules with High Steady State Power and Thermal Stability *J. Mater. Chem. A* **4** 13125-32
[164] Gong J, Darling S B and You F Q 2015 Perovskite Photovoltaics: Life-Cycle Assessment of Energy and Environmental Impacts *Energy Environ. Sci.* **8** 1953-68

[165] Kim J, Yun J S, Cho Y, Lee D S, Wilkinson B, Soufiani A M, Deng X, Zheng J, Shi A, Lim S, Chen S, Hameiri Z, Zhang M, Lau C F J, Huang S, Green M A and Ho-Baillie A W Y 2017 Overcoming the Challenges of Large-Area High-Efficiency Perovskite Solar Cells *ACS Energy Lett.* **2** 1978-84

[166] Burschka J, Pellet N, Moon S J, Humphry-Baker R, Gao P, Nazeeruddin M K and Grätzel M 2013 Sequential Deposition as a Route to High-Performance Perovskite-Sensitized Solar Cells *Nature* **499** 316-9

[167] Jeon N J, Noh J H, Kim Y C, Yang W S, Ryu S and Seok S I 2014 Solvent Engineering for High-Performance Inorganic–Organic Hybrid Perovskite Solar Cells *Nat. Mater.* **13** 897-903

[168] Yang W S, Noh J H, Jeon N J, Kim Y C, Ryu S, Seo J and Seok S I 2015 High-Performance Photovoltaic Perovskite Layers Fabricated through Intramolecular Exchange *Science* **348** 1234-7

[169] Saliba M, Matsui T, Seo J-Y, Domanski K, Correa-Baena J-P, Nazeeruddin M K, Zakeeruddin S M, Tress W, Abate A, Hagfeldt A and Gratzel M 2016 Cesium-Containing Triple Cation Perovskite Solar Cells: Improved Stability, Reproducibility and High Efficiency *Energy Environ. Sci.* **9** 1989-97

[170] Kubicki D J, Prochowicz D, Hofstetter A, Zakeeruddin S M, Gratzel M and Emsley L 2017 Phase Segregation in Cs-, Rb- and K-Doped Mixed-Cation $(MA)_x(FA)_{1-x}PbI_3$ Hybrid Perovskites from Solid-State NMR *J. Am. Chem. Soc.* **139** 14173-80

[171] Son D-Y, Lee J-W, Choi Y J, Jang I-H, Lee S, Yoo P J, Shin H, Ahn N, Choi M, Kim D and Park N-G 2016 Self-Formed Grain Boundary Healing Layer for Highly Efficient $CH_3NH_3PbI_3$ Perovskite Solar Cells *Nat. Energy* **1** 16081

[172] Lee M V, Raga S R, Kato Y, Leyden M R, Ono L K, Wang S and Qi Y 2017 Transamidation of Dimethylformamide during Alkylammonium Lead Triiodide Film Formation for Perovskite Solar Cells *J. Mater. Res.* **32** 45-55

[173] Raga S R, Jung M-C, Lee M V, Leyden M R, Kato Y and Qi Y B 2015 Influence of Air Annealing on High Efficiency Planar Structure Perovskite Solar Cells *Chem. Mater.* **27** 1597-603

[174] Lee L, Baek J, Park K S, Lee Y-E, Shrestha N K and Sung M M 2017 Wafer-scale single-crystal perovskite patterned thin films based on geometrically-confined lateral crystal growth *Nat. Commun.* **8** 15882

[175] Peng W, Yin J, Ho K-T, Ouellette O, De Bastiani M, Murali B, El Tall O, Shen C, Miao X, Pan J, Alarousu E, He J-H, Ooi B S, Mohammed O F, Sargent E and Bakr O M 2017 Ultralow Self-Doping in Two-dimensional Hybrid Perovskite Single Crystals *Nano Lett.* **17** 4759-67

[176] Zhao J, Kong G, Chen S, Li Q, Huang B, Liu Z, San X, Wang Y, Wang C, Zhen Y, Wen H, Gao P and Li J 2017 Single crystalline $CH_3NH_3PbI_3$ self-grown on FTO/TiO_2 substrate for high efficiency perovskite solar cells *Sci. Bull.* **62** 1173-6

[177] Peng W, Wang L, Murali B, Ho K-T, Bera A, Cho N, Kang C-F, Burlakov V M, Pan J, Sinatra L, Ma C, Xu W, Shi D, Alarousu E, Goriely A, He J-H, Mohammed O F, Wu T and Bakr O M 2016 Solution-Grown Monocrystalline Hybrid Perovskite Films for Hole-Transporter-Free Solar Cells *Adv. Mater.* **28** 3383-90

[178] Shi D, Adinolfi V, Comin R, Yuan M, Alarousu E, Buin A, Chen Y, Hoogland S, Rothenberger A, Katsiev K, Losovyj Y, Zhang X, Dowben P A, Mohammed O F, Sargent E H and Bakr O M 2015 Low Trap-State Density and Long Carrier Diffusion in Organolead Trihalide Perovskite Single Crystals *Science* **347** 519-22

[179] Dong Q, Fang Y, Shao Y, Mulligan P, Qiu J, Cao L and Huang J 2015 Electron-Hole Diffusion Lengths > 175 μm in Solution-Grown $CH_3NH_3PbI_3$ Single Crystals *Science* **347** 967-70

[180] Saidaminov M I, Abdelhady A L, Murali B, Alarousu E, Burlakov V M, Peng W, Dursun I, Wang L, He Y, Maculan G, Goriely A, Wu T, Mohammed O F and Bakr O M 2015 High-Quality Bulk Hybrid Perovskite Single Crystals within Minutes by Inverse Temperature Crystallization *Nat. Commun.* **6** 7586
[181] Liu Y, Yang Z, Cui D, Ren X, Sun J, Liu X, Zhang J, Wei Q, Fan H, Yu F, Zhang X, Zhao C and Liu S 2015 Two-Inch-Sized Perovskite $CH_3NH_3PbX_3$ (X = Cl, Br, I) Crystals: Growth and Characterization *Adv. Mater.* **27** 5176-83
[182] Kadro J M, Nonomura K, Gachet D, Grätzel M and Hagfeldt A 2015 Facile route to freestanding $CH_3NH_3PbI_3$ crystals using inverse solubility *Sci. Rep.* **5** 11654
[183] Zhang T, Yang M, Benson E E, Li Z, van de Lagemaat J, Luther J M, Yan Y, Zhu K and Zhao Y 2015 A Facile Solvothermal Growth of Single Crystal Mixed Halide Perovskite $CH_3NH_3Pb(Br_{1-x}Cl_x)_3$ *Chem. Commun.* **51** 7820-3
[184] Lee M M, Teuscher J, Miyasaka T, Murakami T N and Snaith H J 2012 Efficient Hybrid Solar Cells Based on Meso-Superstructured Organometal Halide Perovskites *Science* **338** 643-7
[185] Shin S S, Yeom E J, Yang W S, Hur S, Kim M G, Im J, Seo J, Noh J H and Seok S I 2017 Colloidally Prepared La-Doped $BaSnO_3$ Electrodes for Efficient, Photostable Perovskite Solar Cells *Science* **356** 167-71
[186] Arora N, Dar M I, Hinderhofer A, Pellet N, Schreiber F, Zakeeruddin S M and Grätzel M 2017 Perovskite solar cells with CuSCN hole extraction layers yield stabilized efficiencies greater than 20% *Science* DOI: 10.1126/science.aam5655
[187] Chen H, Ye F, Tang W, He J, Yin M, Wang Y, Xie F, Bi E, Yang X, Gratzel M and Han L 2017 A solvent- and vacuum-free route to large-area perovskite films for efficient solar modules *Nature* **550** 92-5
[188] Yang W S, Park B-W, Jung E H, Jeon N J, Kim Y C, Lee D U, Shin S S, Seo J, Kim E K, Noh J H and Seok S I 2017 Iodide management in formamidinium-lead-halide–based perovskite layers for efficient solar cells *Science* **356** 1376-9
[189] Bush K A, Palmstrom A F, Yu Z J, Boccard M, Cheacharoen R, Mailoa J P, McMeekin D P, Hoye R L Z, Bailie C D, Leijtens T, Peters I M, Minichetti M C, Rolston N, Prasanna R, Sofia S, Harwood D, Ma W, Moghadam F, Snaith H J, Buonassisi T, Holman Z C, Bent S F and McGehee M D 2017 23.6%-Efficient Monolithic Perovskite/Silicon Tandem Solar Cells with Improved Stability *Nat. Energy* **2** 17009
[190] Li X, Bi D, Yi C, Décoppet J-D, Luo J, Zakeeruddin S M, Hagfeldt A and Grätzel M 2016 A Vacuum Flash–Assisted Solution Process for High-Efficiency Large-Area Perovskite Solar Cells *Science* **353** 58-62
[191] Yang M, Zhou Y, Zeng Y, Jiang C-S, Padture N P and Zhu K 2015 Square-Centimeter Solution-Processed Planar $CH_3NH_3PbI_3$ Perovskite Solar Cells with Efficiency Exceeding 15% *Adv. Mater.* **27** 6363-70
[192] Chen W, Wu Y, Yue Y, Liu J, Zhang W, Yang X, Chen H, Bi E, Ashraful I, Grätzel M and Han L 2015 Efficient and stable large-area perovskite solar cells with inorganic charge extraction layers *Science* **350** 944-8
[193] Yang M, Li Z, Reese M O, Reid O G, Kim D H, Siol S, Klein T R, Yan Y, Berry J J, van Hest M F A M and Zhu K 2017 Perovskite Ink with Wide Processing Window for Scalable High-Efficiency Solar Cells *Nat. Energy* **2** 17038
[194] Hu Y, Si S, Mei A, Rong Y, Liu H, Li X and Han H 2017 Stable Large-Area (10×10 cm^2) Printable Mesoscopic Perovskite Module Exceeding 10% Efficiency *Solar RRL* **1** 1600019
[195] Shen P-S, Chen J-S, Chiang Y-H, Li M-H, Guo T-F and Chen P 2016 Low-Pressure Hybrid Chemical Vapor Growth for Efficient Perovskite Solar Cells and Large-Area Module *Adv. Mater. Interfaces* **3** 1500849

[196] Razza S, Castro-Hermosa S, Carlo A D and Brown T M 2016 Research Update: Large-Area Deposition, Coating, Printing, and Processing Techniques for the Upscaling of Perovskite Solar Cell Technology *APL Mater.* **4** 091508
[197] Razza S, Di Giacomo F, Matteocci F, Cinà L, Palma A L, Casaluci S, Cameron P, D'Epifanio A, Licoccia S, Reale A, Brown T M and Di Carlo A 2015 Perovskite solar cells and large area modules (100 cm^2) based on an air flow-assisted PbI_2 blade coating deposition process *J. Power Sources* **277** 286-91
[198] Vak D, Hwang K, Faulks A, Jung Y-S, Clark N, Kim D-Y, Wilson G J and Watkins S E 2015 3D Printer Based Slot-Die Coater as a Lab-to-Fab Translation Tool for Solution-Processed Solar Cells *Adv. Energy Mater.* **5** 1401539
[199] Fakharuddin A, Di Giacomo F, Palma A L, Matteocci F, Ahmed I, Razza S, D'Epifanio A, Licoccia S, Ismail J, Di Carlo A, Brown T M and Jose R 2015 Vertical TiO_2 Nanorods as a Medium for Stable and High-Efficiency Perovskite Solar Modules *ACS Nano* **9** 8420-9
[200] Matteocci F, Razza S, Di Giacomo F, Casaluci S, Mincuzzi G, Brown T M, D'Epifanio A, Licoccia S and Di Carlo A 2014 Solid-state solar modules based on mesoscopic organometal halide perovskite: a route towards the up-scaling process **16** 3918-23
[201] Seo J, Park S, Chan Kim Y, Jeon N J, Noh J H, Yoon S C and Seok S I 2014 Benefits of Very Thin PCBM and LiF Layers for Solution-Processed p-i-n Perovskite Solar Cells *Energy Environ. Sci.* **7** 2642-6
[202] Remeika M and Qi Y 2017 Scalable solution coating of the absorber for perovskite solar cells *J. Energy Chem.*
[203] Remeika M, Raga S R, Zhang S and Qi Y B 2017 Transferrable Optimization of Spray-Coated PbI_2 Films for Perovskite Solar Cell Fabrication *J. Mater. Chem. A* **5** 5709-18
[204] Remeika M, Ono L K, Maeda M, Hu Z and Qi Y 2017 High-throughput surface preparation for flexible slot die coated perovskite solar cells *Org. Electron.* DOI: 10.1016/j.orgel.2017.12.027
[205] Grancini G, Roldán-Carmona C, Zimmermann I, Mosconi E, Lee X, Martineau D, Narbey S, Oswald F, De Angelis F, Graetzel M and Nazeeruddin M K 2017 One-Year stable perovskite solar cells by 2D/3D interface engineering *Nat. Commun.* **8** 15684
[206] Zhou Y, Game O S, Pang S and Padture N P 2015 Microstructures of Organometal Trihalide Perovskites for Solar Cells: Their Evolution from Solutions and Characterization *J. Phys. Chem. Lett.* **6** 4827-39
[207] Park S J, Kim A R, Hong J T, Park J Y, Lee S and Ahn Y H 2017 Crystallization Kinetics of Lead Halide Perovskite Film Monitored by In Situ Terahertz Spectroscopy *J. Phys. Chem. Lett.* **8** 401-6
[208] Munir R, Sheikh A D, Abdelsamie M, Hu H, Yu L, Zhao K, Kim T, Tall O E, Li R, Smilgies D-M and Amassian A 2017 Hybrid Perovskite Thin-Film Photovoltaics: In Situ Diagnostics and Importance of the Precursor Solvate Phases *Adv. Mater.* **29** 1604113
[209] Miyadera T, Shibata Y, Koganezawa T, Murakami T N, Sugita T, Tanigaki N and Chikamatsu M 2015 Crystallization Dynamics of Organolead Halide Perovskite by Real-Time X-ray Diffraction *Nano Lett.* **15** 5630-4
[210] Ham S, Choi Y J, Lee J-W, Park N-G and Kim D 2017 Impact of Excess CH_3NH_3I on Free Carrier Dynamics in High-Performance Nonstoichiometric Perovskites *J. Phys. Chem. C* **121** 3143-8
[211] Kanemitsu Y 2017 Luminescence spectroscopy of lead-halide perovskites: materials properties and application as photovoltaic devices *J. Mater. Chem. C* **5** 3427-37
[212] Soufiani A M, Hameiri Z, Meyer S, Lim S, Tayebjee M J Y, Yun J S, Ho-Baillie A, Conibeer G J, Spiccia L and Green M A 2017 Lessons Learnt from Spatially Resolved

Electro- and Photoluminescence Imaging: Interfacial Delamination in $CH_3NH_3PbI_3$ Planar Perovskite Solar Cells upon Illumination *Adv. Energy Mater.* **7** 1602111

[213] Soufiani A M, Tayebjee M J Y, Meyer S, Ho-Baillie A, Yun J S, MacQueen R W, Spiccia L, Green M A and Hameiri Z 2016 Electro- and photoluminescence imaging as fast screening technique of the layer uniformity and device degradation in planar perovskite solar cells *J. Appl. Phys.* **120** 035702

[214] El-Hajje G, Momblona C, Gil-Escrig L, Avila J, Guillemot T, Guillemoles J-F, Sessolo M, Bolink H J and Lombez L 2016 Quantification of Spatial Inhomogeneity in Perovskite Solar Cells by Hyperspectral Luminescence Imaging *Energy Environ. Sci.* **9** 2286-94

[215] Eperon G E, Moerman D and Ginger D S 2016 Anticorrelation between Local Photoluminescence and Photocurrent Suggests Variability in Contact to Active Layer in Perovskite Solar Cells *ACS Nano* **10** 10258-66

[216] Hameiri Z, Mahboubi Soufiani A, Juhl M K, Jiang L, Huang F, Cheng Y-B, Kampwerth H, Weber J W, Green M A and Trupke T 2015 Photoluminescence and electroluminescence imaging of perovskite solar cells *Prog. Photovolt. Res. Appl.* **23** 1697-705

[217] Mastroianni S, Heinz F D, Im J H, Veurman W, Padilla M, Schubert M C, Wurfel U, Gratzel M, Park N G and Hinsch A 2015 Analysing the effect of crystal size and structure in highly efficient CH3NH3PbI3 perovskite solar cells by spatially resolved photo- and electroluminescence imaging *Nanoscale* **7** 19653-62

[218] Song Z, Werner J, Shrestha N, Sahli F, De Wolf S, Niesen B, Watthage S C, Phillips A B, Ballif C, Ellingson R J and Heben M J 2016 Probing Photocurrent Nonuniformities in the Subcells of Monolithic Perovskite/Silicon Tandem Solar Cells *J. Phys. Chem. Lett.* **7** 5114-20

[219] Jiang Y, Juarez-Perez E J, Ge Q, Wang S, Leyden M R, Ono L K, Raga S R, Hu J and Qi Y 2016 Post-Annealing of $MAPbI_3$ Perovskite Films with Methylamine for Efficient Perovskite Solar Cells *Mater. Horiz.* **3** 548-55

[220] Raga S R, Ono L K and Qi Y B 2016 Rapid Perovskite Formation by CH_3NH_2 Gas-Induced Intercalation and Reaction of PbI_2 *J. Mater. Chem. A* **4** 2494-500

[221] Zong Y, Zhou Y, Ju M, Garces H F, Krause A R, Ji F, Cui G, Zeng X C, Padture N P and Pang S 2016 Thin-Film Transformation of NH_4PbI_3 to $CH_3NH_3PbI_3$ Perovskite: A Methylamine-Induced Conversion–Healing Process *Angew. Chem. Int. Ed.* **55** 14723-7

[222] Pang S, Zhou Y, Wang Z, Yang M, Krause A R, Zhou Z, Zhu K, Padture N P and Cui G 2016 Transformative Evolution of Organolead Triiodide Perovskite Thin Films from Strong Room-Temperature Solid–Gas Interaction between $HPbI_3$-CH_3NH_2 Precursor Pair *J. Am. Chem. Soc.* **138** 750-3

[223] Zhou Z, Wang Z, Zhou Y, Pang S, Wang D, Xu H, Liu Z, Padture N P and Cui G 2015 Methylamine-Gas-Induced Defect-Healing Behavior of $CH_3NH_3PbI_3$ Thin Films for Perovskite Solar Cells *Angew. Chem. Int. Ed.* **54** 9705-9

[224] Zhao Y and Zhu K 2014 Optical bleaching of perovskite (CH3NH3)PbI3 through room-temperature phase transformation induced by ammonia *Chem. Commun.* **50** 1605-7

[225] Zhang T, Guo N, Li G, Qian X, Li L and Zhao Y 2016 A general non-CH_3NH_3X (X = I, Br) one-step deposition of $CH_3NH_3PbX_3$ perovskite for high performance solar cells *J. Mater. Chem. A* **4** 3245-8

[226] Zhang T, Li G, Xu F, Wang Y, Guo N, Qian X and Zhao Y 2016 In situ Gas/Solid Reaction for the Formation of Luminescent Quantum Confined $CH_3NH_3PbBr_3$ Perovskite Planar Film *Chem. Commun.* **52** 11080-3

[227] Chih Y-K, Wang J-C, Yang R-T, Liu C-C, Chang Y-C, Fu Y-S, Lai W-C, Chen P, Wen T-C, Huang Y-C, Tsao C-S and Guo T-F 2016 NiO_x Electrode Interlayer and $CH_3NH_2/CH_3NH_3PbBr_3$ Interface Treatment to Markedly Advance Hybrid Perovskite-Based Light-Emitting Diodes *Adv. Mater.* **28** 8687-94
[228] Liu Z, Hu J, Jiao H, Li L, Zheng G, Chen Y, Huang Y, Zhang Q, Shen C, Chen Q and Zhou H 2017 Chemical Reduction of Intrinsic Defects in Thicker Heterojunction Planar Perovskite Solar Cells *Adv. Mater.* **29** 1606774
[229] Noel N K, Habisreutinger S N, Wenger B, Klug M T, Horantner M T, Johnston M B, Nicholas R J, Moore D T and Snaith H J 2017 A Low Viscosity, Low Boiling Point, Clean Solvent System for the Rapid Crystallisation of Highly Specular Perovskite Films *Energy Environ. Sci.* **10** 145-52
[230] Liu M Z, Johnston M B and Snaith H J 2013 Efficient Planar Heterojunction Perovskite Solar Cells by Vapour Deposition *Nature* **501** 395-8
[231] Malinkiewicz O, Yella A, Lee Y H, Espallargas G M, Graetzel M, Nazeeruddin M K and Bolink H J 2014 Perovskite solar cells employing organic charge-transport layers *Nat. Photonics* **8** 128-32
[232] Ono L K, Wang S, Kato Y, Raga S R and Qi Y B 2014 Semi-Transparent Perovskite Films with Centimeter-scale Superior Uniformity by the Hybrid Deposition Method *Energy Environ. Sci.* **7** 3989-93
[233] Sessolo M, Momblona C, Gil-Escrig L and Bolink H J 2015 Photovoltaic devices employing vacuum-deposited perovskite layers *MRS Bulletin* **40** 660-6
[234] Wang S, Ono L K, Leyden M R, Kato Y, R. Raga S, Lee M V and Qi Y B 2015 Smooth Perovskite Thin Films and Efficient Perovskite Solar Cells Prepared by the Hybrid Deposition Method *J. Mater. Chem. A* **3** 14631-41
[235] Ávila J, Momblona C, Boix P P, Sessolo M and Bolink H J 2017 Vapor-Deposited Perovskites: The Route to High-Performance Solar Cell Production? *Joule* DOI: 10.1016/j.joule.2017.07.014
[236] Leyden M R, Meng L, Jiang Y, Ono L K, Qiu L, Juarez-Perez E J, Qin C, Adachi C and Qi Y 2017 Methylammonium Lead Bromide Perovskite Light-Emitting Diodes by Chemical Vapor Deposition *J. Phys. Chem. Lett.* **8** 3193-8
[237] Leyden M R, Lee M V, Raga S R and Qi Y B 2015 Large Formamidinium Lead Trihalide Perovskite Solar Cells Using Chemical Vapor Deposition with High Reproducibility and Tunable Chlorine Concentrations *J. Mater. Chem. A* **3** 16097-103
[238] Leyden M R, Ono L K, Raga S R, Kato Y, Wang S H and Qi Y B 2014 High Performance Perovskite Solar Cells by Hybrid Chemical Vapor Deposition *J. Mater. Chem. A* **2** 18742-5
[239] Jiang Y, Leyden M R, Qiu L, Wang S, Ono L K, Wu Z, Juarez-Perez E J and Qi Y B 2017 Combination of Hybrid CVD and Cation Exchange for Up-Scaling Cs-Substituted Mixed Cation Perovskite Solar Cells with High Efficiency and Stability *Adv. Func. Mater.* **27** 1703835
[240] Kim D H, Park J, Li Z, Yang M, Park J-S, Park I J, Kim J Y, Berry J J, Rumbles G and Zhu K 2017 300% Enhancement of Carrier Mobility in Uniaxial-Oriented Perovskite Films Formed by Topotactic-Oriented Attachment *Adv. Mater.* **29** 1606831
[241] Tsai C-M, Wu G-W, Narra S, Chang H-M, Mohanta N, Wu H-P, Wang C-L and Diau E W-G 2017 Control of Preferred Orientation with Slow Crystallization for Carbon-Based Mesoscopic Perovskite Solar Cells Attaining Efficiency 15% *J. Mater. Chem. A* **5** 739-47
[242] Foley B J, Girard J, Sorenson B A, Chen A Z, Scott Niezgoda J, Alpert M R, Harper A F, Smilgies D-M, Clancy P, Saidi W A and Choi J J 2017 Controlling Nucleation,

Growth, and Orientation of Metal Halide Perovskite Thin Films with Rationally Selected Additives *J. Mater. Chem. A* **5** 113-23

[243] Bai Y, Xiao S, Hu C, Zhang T, Meng X, Li Q, Yang Y, Wong K S, Chen H and Yang S 2017 A Pure and Stable Intermediate Phase is Key to Growing Aligned and Vertically Monolithic Perovskite Crystals for Efficient PIN Planar Perovskite Solar Cells with High Processibility and Stability *Nano Energy* **34** 58-68

[244] Cho N, Li F, Turedi B, Sinatra L, Sarmah S P, Parida M R, Saidaminov M I, Murali B, Burlakov V M, Goriely A, Mohammed O F, Wu T and Bakr O M 2016 Pure Crystal Orientation and Anisotropic Charge Transport in Large-Area Hybrid Perovskite Films *Nat. Commun.* **7** 13407

[245] Chen H, Zheng X, Li Q, Yang Y, Xiao S, Hu C, Bai Y, Zhang T, Wong K S and Yang S 2016 An Amorphous Precursor Route to the Conformable Oriented Crystallization of $CH_3NH_3PbBr_3$ in Mesoporous Scaffolds: Toward Efficient and Thermally Stable Carbon-Based Perovskite Solar Cells *J. Mater. Chem. A* **4** 12897-912

[246] Ng A, Ren Z, Shen Q, Cheung S H, Gokkaya H C, So S K, Djurišić A B, Wan Y, Wu X and Surya C 2016 Crystal Engineering for Low Defect Density and High Efficiency Hybrid Chemical Vapor Deposition Grown Perovskite Solar Cells *ACS Appl. Mater. Interfaces* **8** 32805-14

[247] Tavakoli M M, Gu L, Gao Y, Reckmeier C, He J, Rogach A L, Yao Y and Fan Z 2015 Fabrication of efficient planar perovskite solar cells using a one-step chemical vapor deposition method *Sci. Rep.* **5** 14083

[248] Luo P F, Liu Z F, Xia W, Yuan C C, Cheng J G and Lu Y W 2015 A simple in situ tubular chemical vapor deposition processing of large-scale efficient perovskite solar cells and the research on their novel roll-over phenomenon in J-V curves *J. Mater. Chem. A* **3** 12443-51

[249] Luo P F, Liu Z F, Xia W, Yuan C C, Cheng J G and Lu Y W 2015 Uniform, Stable, and Efficient Planar-Heterojunction Perovskite Solar Cells by Facile Low-Pressure Chemical Vapor Deposition under Fully Open-Air Conditions *ACS Appl. Mater. Interfaces* **7** 2708-14

[250] Wang B and Chen T 2015 Exceptionally Stable $CH_3NH_3PbI_3$ Films in Moderate Humid Environmental Condition *Adv. Sci.* **2** 1500262

[251] Peng Y K, Jing G S and Cui T H 2015 A hybrid physical-chemical deposition process at ultra-low temperatures for high-performance perovskite solar cells *J. Mater. Chem. A* **3** 12436-42

[252] Domanski K, Correa-Baena J-P, Mine N, Nazeeruddin M K, Abate A, Saliba M, Tress W, Hagfeldt A and Grätzel M 2016 Not All That Glitters Is Gold: Metal-Migration-Induced Degradation in Perovskite Solar Cells *ACS Nano* **10** 6306-14

[253] Leijtens T, Bush K, Cheacharoen R, Beal R, Bowring A and McGehee M D 2017 Towards Enabling Stable Lead Halide Perovskite Solar Cells; Interplay Between Structural, Environmental, and Thermal Stability *J. Mater. Chem. A* **5** 11483-500

[254] Asghar M I, Zhang J, Wang H and Lund P D 2017 Device stability of perovskite solar cells – A review *Renew. Sustain. Energy Rev.* **77** 131-46

[255] Wu Z, Raga S R, Juarez-Perez E J, Yao X, Jiang Y, Ono L K, Ning Z, Tian H and Qi Y B 2017 Improved Efficiency and Stability of Perovskite Solar Cells Induced by C=O Functionalized Hydrophobic Ammonium-Based Additives *Adv. Mater.* **29** 1703670

[256] Conings B, Drijkoningen J, Gauquelin N, Babayigit A, D'Haen J, D'Olieslaeger L, Ethirajan A, Verbeeck J, Manca J, Mosconi E, Angelis F D and Boyen H-G 2015 Intrinsic Thermal Instability of Methylammonium Lead Trihalide Perovskite *Adv. Energy Mater.* **5** 1500477

[257] Osterwald C R and McMahon T J 2009 History of Accelerated and Qualification Testing of Terrestrial Photovoltaic Modules: A Literature Review *Prog. Photovolt. Res. Appl.* **17** 11-33
[258] Bag M, Renna L A, Adhikari R Y, Karak S, Liu F, Lahti P M, Russell T P, Tuominen M T and Venkataraman D 2015 Kinetics of Ion Transport in Perovskite Active Layers and Its Implications for Active Layer Stability *J. Am. Chem. Soc.* **137** 13130-7
[259] Milot R L, Eperon G E, Snaith H J, Johnston M B and Herz L M 2015 Temperature-Dependent Charge-Carrier Dynamics in CH3NH3PbI3 Perovskite Thin Films *Adv. Func. Mater.* **25** 6218-27
[260] Zhang H, Qiao X, Shen Y and Wang M 2015 Effect of temperature on the efficiency of organometallic perovskite solar cells *J. Energy Chem.* **24** 729
[261] Zhang H, Qiao X, Shen Y, Moehl T, Zakeeruddin S M, Gratzel M and Wang M 2015 Photovoltaic behaviour of lead methylammonium triiodide perovskite solar cells down to 80 K *J. Mater. Chem. A* **3** 11762-7
[262] Wang M, Yim W-L, Liao P and Shen Y 2017 Temperature Dependent Characteristics of Perovskite Solar Cells *ChemSelect* **2** 4469-77
[263] Manser J S, Saidaminov M I, Christians J A, Bakr O M and Kamat P V 2016 Making and Breaking of Lead Halide Perovskites *Acc. Chem. Res.* **49** 330-8
[264] Juarez-Perez E J, Hawash Z, Raga S R, Ono L K and Qi Y B 2016 Thermal Degradation of $CH_3NH_3PbI_3$ Perovskite into NH_3 and CH_3I Gases Observed by Coupled Thermogravimetry-Mass Spectrometry Analysis *Energy Environ. Sci.* **9** 3406-10
[265] Latini A, Gigli G and Ciccioli A 2017 A study on the nature of the thermal decomposition of methylammonium lead iodide perovskite, $CH_3NH_3PbI_3$: an attempt to rationalise contradictory experimental results *Sustain. Energy Fuels* **1** 1351-7
[266] Jung M-C, Lee Y M, Lee H-K, Park J, Raga S R, Ono L K, Wang S, Leyden M R, Yu B D, Hong S and Qi Y B 2016 The Presence of CH_3NH_2 Neutral Species in Organometal Halide Perovskite Films *Appl. Phys. Lett.* **108** 073901
[267] Xu F, Zhang T, Li G and Zhao Y 2017 Mixed Cation Hybrid Lead Halide Perovskites with Enhanced Performance and Stability *J. Mater. Chem. A* **5** 11450-61
[268] Xu T, Chen L, Guo Z and Ma T 2016 Strategic Improvement of The Long-Term Stability of Perovskite Materials and Perovskite Solar Cells *Phys. Chem. Chem. Phys.* **18** 27026-50
[269] Berhe T A, Su W-N, Chen C-H, Pan C-J, Cheng J-H, Chen H-M, Tsai M-C, Chen L-Y, Dubale A A and Hwang B-J 2016 Organometal Halide Perovskite Solar Cells: Degradation and Stability *Energy Environ. Sci.* **9** 323-56
[270] Habisreutinger S N, McMeekin D P, Snaith H J and Nicholas R J 2016 Research Update: Strategies for Improving The Stability of Perovskite Solar Cells *APL Mater.* **4** 091503
[271] Wang S, Jiang Y, Juarez-Perez Emilio J, Ono L K and Qi Y B 2016 Accelerated Degradation of Methylammonium Lead Iodide Perovskites Induced by Exposure to Iodine Vapour *Nat. Energy* **2** 16195
[272] Wilks R G and Bär M 2017 Perovskite solar cells: Danger from within *Nat. Energy* **2** 16204
[273] Kato Y, Ono L K, Lee M V, Wang S H, Raga S R and Qi Y B 2015 Silver Iodide Formation in Methyl Ammonium Lead Iodide Perovskite Solar Cells with Silver Top Electrodes *Adv. Mater. Interfaces* **2** 1500195
[274] Zhou Y, Zhou Z, Chen M, Zong Y, Huang J, Pang S and Padture N P 2016 Doping and alloying for improved perovskite solar cells *J. Mater. Chem. A* **4** 17623-35

[275] Guerrero A, You J, Aranda C, Kang Y S, Garcia-Belmonte G, Zhou H, Bisquert J and Yang Y 2016 Interfacial Degradation of Planar Lead Halide Perovskite Solar Cells *ACS Nano* **10** 218-24
[276] Cacovich S, Divitini G, Ireland C, Matteocci F, Di Carlo A and Ducati C 2016 Elemental Mapping of Perovskite Solar Cells by Using Multivariate Analysis: An Insight into Degradation Processes *Chem. Sus. Chem.* **9** 2673-8
[277] Divitini G, Cacovich S, Matteocci F, Cinà L, Di Carlo A and Ducati C 2016 In situ Observation of Heat-Induced Degradation of Perovskite Solar Cells *Nat. Energy* **1** 15012
[278] Kaltenbrunner M, Adam G, Glowacki E D, Drack M, Schwodiauer R, Leonat L, Apaydin D H, Groiss H, Scharber M C, White M S, Sariciftci N S and Bauer S 2015 Flexible high power-per-weight perovskite solar cells with chromium oxide-metal contacts for improved stability in air *Nat. Mater.* **14** 1032
[279] Akbari A, Hashemi J, Mosconi E, De Angelis F and Hakala M 2017 First principles modelling of perovskite solar cells based on TiO_2 and $Al2O_3$: stability and interfacial electronic structure *J. Mater. Chem. A* **5** 2339-45
[280] Zuo L, Chen Q, De Marco N, Hsieh Y-T, Chen H, Sun P, Chang S-Y, Zhao H, Dong S and Yang Y 2017 Tailoring the Interfacial Chemical Interaction for High-Efficiency Perovskite Solar Cells *Nano Lett.* **17** 269-75
[281] Qiu L, Ono L K, Jiang Y, Leyden M R, Raga S R, Wang S and Qi Y 2017 Engineering Interface Structure to Improve Efficiency and Stability of Organometal Halide Perovskite Solar Cells *J. Phys. Chem. B* DOI: 10.1021/acs.jpcb.7b03921
[282] Shi J, Xu X, Li D and Meng Q 2015 Interfaces in Perovskite Solar Cells *Small* **11** 2472-86
[283] Qin C, Matsushima T, Fujihara T, Potscavage W J and Adachi C 2016 Degradation Mechanisms of Solution-Processed Planar Perovskite Solar Cells: Thermally Stimulated Current Measurement for Analysis of Carrier Traps *Adv. Mater.* **28** 466-71
[284] Qin C, Matsushima T, Fujihara T and Adachi C 2017 Multifunctional Benzoquinone Additive for Efficient and Stable Planar Perovskite Solar Cells *Adv. Mater.* **29** 1603808
[285] Mahmood K, Sarwar S and Mehran M T 2017 Current Status of Electron Transport Layers in Perovskite Solar Cells: Materials and Properties *RSC Adv.* **7** 17044-62
[286] Thakur U, Kisslinger R and Shankar K 2017 One-Dimensional Electron Transport Layers for Perovskite Solar Cells *Nanomater.* **7** 95
[287] Yang G, Tao H, Qin P, Ke W and Fang G 2016 Recent Progress in Electron Transport Layers for Efficient Perovskite Solar Cells *J. Mater. Chem. A* **4** 3970-90
[288] Leijtens T, Eperon G E, Pathak S, Abate A, Lee M M and Snaith H J 2013 Overcoming ultraviolet light instability of sensitized TiO_2 with meso-superstructured organometal tri-halide perovskite solar cells *Nat Commun* **4** 2885
[289] Pham H D, Wu Z, Ono L K, Manzhos S, Feron K, Motta N, Qi Y and Sonar P 2017 Low-Cost Alternative High-Performance Hole-Transport Material for Perovskite Solar Cells and Its Comparative Study with Conventional SPIRO-OMeTAD *Adv. Electron. Mater.* **3** 1700139
[290] Ameen S, Rub M A, Kosa S A, Alamry K A, Akhtar M S, Shin H-S, Seo H-K, Asiri A M and Nazeeruddin M K 2016 Perovskite Solar Cells: Influence of Hole Transporting Materials on Power Conversion Efficiency *Chem. Sus. Chem.* **9** 10-27
[291] Calió L, Kazim S, Grätzel M and Ahmad S 2016 Hole-Transport Materials for Perovskite Solar Cells *Angew. Chem. Int. Ed.* **55** 14522-45
[292] Lin Q, Armin A, Burn P L and Meredith P 2016 Organohalide Perovskites for Solar Energy Conversion *Acc. Chem. Res.* **49** 545-53

[293] Jung M-C and Qi Y B 2016 Dopant Interdiffusion Effects in n-i-p Structured Spiro-OMeTAD Hole Transport Layer of Organometal Halide Perovskite Solar Cells *Org. Electron.* **31** 71-6
[294] Jung M C, Raga S R, Ono L K and Qi Y B 2015 Substantial Improvement of Perovskite Solar Cells Stability by Pinhole-Free Hole Transport Layer with Doping Engineering *Sci. Rep.* **5** 9863
[295] Hawash Z, Ono L K, Raga S R, Lee M V and Qi Y B 2015 Air-Exposure Induced Dopant Redistribution and Energy Level Shifts in Spin-Coated Spiro-MeOTAD Films *Chem. Mater.* **27** 562-9
[296] Ono L K, Raga S R, Remeika M, Winchester A J, Gabe A and Qi Y B 2015 Pinhole-Free Hole Transport Layers Significantly Improve the Stability of $MAPbI_3$-Based Perovskite Solar Cells Under Operating Conditions *J. Mater. Chem. A* **3** 15451-6
[297] Ono L K, Schulz P, Endres J J, Nikiforov G O, Kato Y, Kahn A and Qi Y B 2014 Air-Exposure-Induced Gas-Molecule Incorporation into Spiro-MeOTAD Films *J. Phys. Chem. Lett.* **5** 1374-9
[298] Hawash Z, Ono L K and Qi Y B 2016 Moisture and Oxygen Enhance Conductivity of LiTFSI-Doped Spiro-MeOTAD Hole Transport Layer in Perovskite Solar Cells *Adv. Mater. Interfaces* **3** 1600117
[299] Juarez-Perez E J, Leyden M R, Wang S, Ono L K, Hawash Z and Qi Y B 2016 Role of the Dopants on the Morphological and Transport Properties of Spiro-MeOTAD Hole Transport Layer *Chem. Mater.* **28** 5702-9
[300] Chen D, Wang D, Yang Y, Huang Q, Zhu S and Zheng Z 2017 Self-Healing Materials for Next-Generation Energy Harvesting and Storage Devices *Adv. Energy Mater.* **7** 1700890
[301] Banerjee S, Tripathy R, Cozzens D, Nagy T, Keki S, Zsuga M and Faust R 2015 Photoinduced Smart, Self-Healing Polymer Sealant for Photovoltaics *ACS Appl. Mater. Interfaces* **7** 2064-72
[302] Bag M, Banerjee S, Faust R and Venkataraman D 2016 Self-healing polymer sealant for encapsulating flexible solar cells *Sol. Energy Mater. Sol. Cells* **145, Part 3** 418-22
[303] Lv T, Cheng Z, Zhang E, Kang H, Liu Y and Jiang L 2017 Self-Restoration of Superhydrophobicity on Shape Memory Polymer Arrays with Both Crushed Microstructure and Damaged Surface Chemistry *Small* **13** 1503402
[304] Zhao Y, Wei J, Li H, Yan Y, Zhou W, Yu D and Zhao Q 2016 A polymer scaffold for self-healing perovskite solar cells *Nat. Commun.* **7** 10228
[305] Wang Z, McMeekin D P, Sakai N, van Reenen S, Wojciechowski K, Patel J B, Johnston M B and Snaith H J 2017 Efficient and Air-Stable Mixed-Cation Lead Mixed-Halide Perovskite Solar Cells with n-Doped Organic Electron Extraction Layers *Adv. Mater.* **29** 1604186
[306] Mesquita I, Andrade L and Mendes A 2017 Perovskite solar cells: Materials, configurations and stability *Renewable Sustainable Energy Rev.* DOI: 10.1016/j.rser.2017.09.011
[307] Ogunseitan O A 2016 Power Failure: The Battered Legacy of Leaded Batteries *Environ. Sci. Technol.* **50** 8401-2
[308] Abate A 2017 Perovskite Solar Cells Go Lead Free DOI: 10.1016/j.joule.2017.09.007
[309] Babayigit A, Duy Thanh D, Ethirajan A, Manca J, Muller M, Boyen H-G and Conings B 2016 Assessing the toxicity of Pb- and Sn-based perovskite solar cells in model organism Danio rerio *Sci. Rep.* **6** 18721
[310] Babayigit A, Ethirajan A, Muller M and Conings B 2016 Toxicity of Organometal Halide Perovskite Solar Cells *Nat. Mater.* **15** 247-51

[311] Jung M-C, Raga S R and Qi Y B 2016 Properties and Solar Cell Applications of Pb-Free Perovskite Films Formed by Vapor Deposition *RSC Adv.* **6** 2819-25
[312] Zhao Z, Gu F, Li Y, Sun W, Ye S, Rao H, Liu Z, Bian Z and Huang C 2017 Mixed-Organic-Cation Tin Iodide for Lead-Free Perovskite Solar Cells with an Efficiency of 8.12% *Adv. Sci.* **4** 1700204
[313] Hoefler S F, Trimmel G and Rath T 2017 Progress on lead-free metal halide perovskites for photovoltaic applications: a review *Monatsh. Chem.* **148** 795-826
[314] Chakraborty S, Xie W, Mathews N, Sherburne M, Ahuja R, Asta M and Mhaisalkar S G 2017 Rational Design: A High-Throughput Computational Screening and Experimental Validation Methodology for Lead-Free and Emergent Hybrid Perovskites *ACS Energy Lett.* **2** 837-45
[315] Shi Z, Guo J, Chen Y, Li Q, Pan Y, Zhang H, Xia Y and Huang W 2017 Lead-Free Organic–Inorganic Hybrid Perovskites for Photovoltaic Applications: Recent Advances and Perspectives *Adv. Mater.* **29** 1605005
[316] Meng W, Wang X, Xiao Z, Wang J, Mitzi D B and Yan Y 2017 Parity-Forbidden Transitions and Their Impact on the Optical Absorption Properties of Lead-Free Metal Halide Perovskites and Double Perovskites *J. Phys. Chem. Lett.* **8** 2999-3007
[317] Xiao Z W, Meng W W, Wang J B, Mitzi D B and Yan Y F 2017 Searching for Promising New Perovskite-Based Photovoltaic Absorbers: The Importance of Electronic Dimensionality *Mater. Horiz.* **4** 206-16
[318] Park B-W, Philippe B, Zhang X, Rensmo H, Boschloo G and Johansson E M J 2015 Bismuth Based Hybrid Perovskites $A_3Bi_2I_9$ (A: Methylammonium or Cesium) for Solar Cell Application *Adv. Mater.* **27** 6806-13
[319] Johansson M B, Zhu H and Johansson E M J 2016 Extended Photo-Conversion Spectrum in Low-Toxic Bismuth Halide Perovskite Solar Cells *J. Phys. Chem. Lett.* **7** 3467-71
[320] Saparov B, Sun J-P, Meng W, Xiao Z, Duan H-S, Gunawan O, Shin D, Hill I G, Yan Y and Mitzi D B 2016 Thin-Film Deposition and Characterization of a Sn-Deficient Perovskite Derivative Cs2SnI6 *Chem. Mater.* **28** 2315-22
[321] Lee B, Stoumpos C C, Zhou N, Hao F, Malliakas C, Yeh C-Y, Marks T J, Kanatzidis M G and Chang R P H 2014 Air-Stable Molecular Semiconducting Iodosalts for Solar Cell Applications: Cs_2SnI_6 as a Hole Conductor *J. Am. Chem. Soc.* **136** 15379-85
[322] Harikesh P C, Mulmudi H K, Ghosh B, Goh T W, Teng Y T, Thirumal K, Lockrey M, Weber K, Koh T M, Li S, Mhaisalkar S and Mathews N 2016 Rb as an Alternative Cation for Templating Inorganic Lead-Free Perovskites for Solution Processed Photovoltaics *Chem. Mater.* **28** 7496-504
[323] Ran C, Wu Z, Xi J, Yuan F, Dong H, Lei T, He X and Hou X 2017 Construction of Compact Methylammonium Bismuth Iodide Film Promoting Lead-Free Inverted Planar Heterojunction Organohalide Solar Cells with Open-Circuit Voltage over 0.8 V *J. Phys. Chem. Lett.* **8** 394-400
[324] Singh T, Kulkarni A, Ikegami M and Miyasaka T 2016 Effect of Electron Transporting Layer on Bismuth-Based Lead-Free Perovskite $(CH_3NH_3)_3$ Bi_2I_9 for Photovoltaic Applications *ACS Appl. Mater. Interfaces* **8** 14542-7
[325] Zhang Z, Li X, Xia X, Wang Z, Huang Z, Lei B and Gao Y 2017 High-Quality $(CH_3NH_3)_3Bi_2I_9$ Film-Based Solar Cells: Pushing Efficiency up to 1.64% *J. Phys. Chem. Lett.* **8** 4300-7
[326] Slavney A H, Hu T, Lindenberg A M and Karunadasa H I 2016 A Bismuth-Halide Double Perovskite with Long Carrier Recombination Lifetime for Photovoltaic Applications *J. Am. Chem. Soc.* **138** 2138-41

[327] McClure E T, Ball M R, Windl W and Woodward P M 2016 Cs_2AgBiX_6 (X = Br, Cl): New Visible Light Absorbing, Lead-Free Halide Perovskite Semiconductors *Chem. Mater.* **28** 1348-54
[328] Wei F, Deng Z, Sun S, Xie F, Kieslich G, Evans D M, Carpenter M A, Bristowe P D and Cheetham A K 2016 The synthesis, structure and electronic properties of a lead-free hybrid inorganic-organic double perovskite $(MA)_2KBiCl_6$ (MA = methylammonium) *Mater. Horiz.* **3** 328-32
[329] Volonakis G, Filip M R, Haghighirad A A, Sakai N, Wenger B, Snaith H J and Giustino F 2016 Lead-Free Halide Double Perovskites via Heterovalent Substitution of Noble Metals *J. Phys. Chem. Lett.* **7** 1254-9
[330] Giustino F and Snaith H J 2016 Toward Lead-Free Perovskite Solar Cells *ACS Energy Lett.* **1** 1233-40
[331] Slavney A H, Smaha R W, Smith I C, Jaffe A, Umeyama D and Karunadasa H I 2017 Chemical Approaches to Addressing the Instability and Toxicity of Lead-Halide Perovskite Absorbers *Inorg. Chem.* **56** 46-55
[332] Zhao X-G, Yang J-H, Fu Y, Yang D, Xu Q, Yu L, Wei S-H and Zhang L 2017 Design of Lead-Free Inorganic Halide Perovskites for Solar Cells via Cation-Transmutation *J. Am. Chem. Soc.* **139** 2630-8
[333] Saparov B and Mitzi D B 2016 Organic–Inorganic Perovskites: Structural Versatility for Functional Materials Design *Chem. Rev.* **116** 4558-96
[334] Savory C N, Walsh A and Scanlon D O 2016 Can Pb-Free Halide Double Perovskites Support High-Efficiency Solar Cells? *ACS Energy Lett.* **1** 949-55
[335] Chen S, Gong X G, Walsh A and Wei S-H 2009 Electronic structure and stability of quaternary chalcogenide semiconductors derived from cation cross-substitution of II-VI and I-III-VI_2 compounds *Phys. Rev. B* **79** 165211
[336] Wallace S K, Mitzi D B and Walsh A 2017 The Steady Rise of Kesterite Solar Cells *ACS Energy Lett.* **2** 776-9
[337] Pan W, Wu H, Luo J, Deng Z, Ge C, Chen C, Jiang X, Yin W-J, Niu G, Zhu L, Yin L, Zhou Y, Xie Q, Ke X, Sui M and Tang J 2017 $Cs_2AgBiBr_6$ single-crystal X-ray detectors with a low detection limit *Nat. Photon.* DOI: 10.1038/s41566-017-0012-4
[338] Volonakis G, Haghighirad A A, Milot R L, Sio W H, Filip M R, Wenger B, Johnston M B, Herz L M, Snaith H J and Giustino F 2017 $Cs_2InAgCl_6$: A New Lead-Free Halide Double Perovskite with Direct Band Gap *J. Phys. Chem. Lett.* **8** 772-8
[339] Wei F, Deng Z, Sun S, Zhang F, Evans D M, Kieslich G, Tominaka S, Carpenter M A, Zhang J, Bristowe P D and Cheetham A K 2017 Synthesis and Properties of a Lead-Free Hybrid Double Perovskite: $(CH_3NH_3)_2AgBiBr_6$ *Chem. Mater.* **29** 1089-94
[340] Nakajima T and Sawada K 2017 Discovery of Pb-Free Perovskite Solar Cells via High-Throughput Simulation on the K Computer *J. Phys. Chem. Lett.* **8** 4826-31
[341] Ju M-G, Dai J, Ma L and Zeng X C 2017 Lead-Free Mixed Tin and Germanium Perovskites for Photovoltaic Application *J. Am. Chem. Soc.* **139** 8038-43
[342] Nazarenko O, Yakunin S, Morad V, Cherniukh I and Kovalenko M V 2017 Single crystals of caesium formamidinium lead halide perovskites: solution growth and gamma dosimetry *NPG Asia Mater.* **9** e373
[343] Yakunin S, Dirin D N, Shynkarenko Y, Morad V, Cherniukh I, Nazarenko O, Kreil D, Nauser T and Kovalenko M V 2016 Detection of Gamma Photons Using Solution-Grown Single Crystals of Hybrid Lead Halide Perovskites *Nat. Photon.* **10** 585-9
[344] Yakunin S, Sytnyk M, Kriegner D, Shrestha S, Richter M, Matt G J, Azimi H, Brabec C J, Stangl J, Kovalenko M V and Heiss W 2015 Detection of X-ray Photons by Solution-Processed Lead Halide Perovskites *Nat. Photon.* **9** 444-9

[345] Wei H, Fang Y, Mulligan P, Chuirazzi W, Fang H-H, Wang C, Ecker B R, Gao Y, Loi M A, Cao L and Huang J 2016 Sensitive X-ray Detectors Made of Methylammonium Lead Tribromide Perovskite Single Crystals *Nat. Photon.* **10** 333-9
[346] Shrestha S, Fischer R, Matt G J, Feldner P, Michel T, Osvet A, Levchuk I, Merle B, Golkar S, Chen H, Tedde S F, Schmidt O, Hock R, Rührig M, Göken M, Heiss W, Anton G and Brabec C J 2017 High-performance direct conversion X-ray detectors based on sintered hybrid lead triiodide perovskite wafers *Nat. Photon.* **11** 436
[347] Wei W, Zhang Y, Xu Q, Wei H, Fang Y, Wang Q, Deng Y, Li T, Gruverman A, Cao L and Huang J 2017 Monolithic integration of hybrid perovskite single crystals with heterogenous substrate for highly sensitive X-ray imaging *Nat. Photon.* **11** 315
[348] Kim Y C, Kim K H, Son D-Y, Jeong D-N, Seo J-Y, Choi Y S, Han I T, Lee S Y and Park N-G 2017 Printable organometallic perovskite enables large-area, low-dose X-ray imaging *Nature* **550** 87-91
[349] Zhou Y and Zhu K 2016 Perovskite Solar Cells Shine in the "Valley of the Sun" *ACS Energy Lett.* **1** 64-7
[350] Bisquert J, Qi Y B, Ma T and Yan Y 2017 Advances and Obstacles on Perovskite Solar Cell Research from Material Properties to Photovoltaic Function *ACS Energy Lett.* **2** 520-3
[351] Bu T, Liu X, Zhou Y, Yi J, Huang X, Luo L, Xiao J, Ku Z, Peng Y, Huang F, Cheng Y-B and Zhong J 2017 Novel quadruple-cation absorber for universal hysteresis elimination for high efficiency and stable perovskite solar cells *Energy Environ. Sci.* DOI: 10.1039/C7EE02634J
[352] Rong Y, Liu L, Mei A, Li X and Han H 2015 Beyond Efficiency: the Challenge of Stability in Mesoscopic Perovskite Solar Cells *Adv. Energy Mater.* **5** 1501066
[353] Misra R K, Aharon S, Li B, Mogilyansky D, Visoly-Fisher I, Etgar L and Katz E A 2015 Temperature- and Component-Dependent Degradation of Perovskite Photovoltaic Materials under Concentrated Sunlight *J. Phys. Chem. Lett.* **6** 326-30
[354] Misra R K, Ciammaruchi L, Aharon S, Mogilyansky D, Etgar L, Visoly-Fisher I and Katz E A 2016 Effect of Halide Composition on the Photochemical Stability of Perovskite Photovoltaic Materials *Chem. Sus. Chem.* **9** 2572-7
[355] Visoly-Fisher I, Mescheloff A, Gabay M, Bounioux C, Zeiri L, Sansotera M, Goryachev A E, Braun A, Galagan Y and Katz E A 2015 Concentrated sunlight for accelerated stability testing of organic photovoltaic materials: towards decoupling light intensity and temperature *Sol. Energy Mater. Sol. Cells* **134** 99-107
[356] Tress W 2017 Perovskite Solar Cells on the Way to Their Radiative Efficiency Limit – Insights Into a Success Story of High Open-Circuit Voltage and Low Recombination *Adv. Energy Mater.* **7** 1602358
[357] Bernardi M and Grossman J C 2016 Computer calculations across time and length scales in photovoltaic solar cells *Energy Environ. Sci.* **9** 2197-218
[358] Yuan Y, Wang Q, Shao Y, Lu H, Li T, Gruverman A and Huang J 2016 Electric-Field-Driven Reversible Conversion Between Methylammonium Lead Triiodide Perovskites and Lead Iodide at Elevated Temperatures *Adv. Energy Mater.* **6** 1501803
[359] Qi Y B 2011 Investigation of Organic Films by Atomic Force Microscopy: Structural, Nanotribological and Electrical Properties *Surf. Sci. Rep.* **66** 379-93
[360] Hieulle J, Stecker C, Ohmann R, Ono L K and Qi Y 2017 Scanning Probe Microscopy Applied to Organic–Inorganic Halide Perovskite Materials and Solar Cells **1** 1700295
[361] Hoye R L Z, Schulz P, Schelhas L T, Holder A M, Stone K H, Perkins J D, Vigil-Fowler D, Siol S, Scanlon D O, Zakutayev A, Walsh A, Smith I C, Melot B C, Kurchin R C, Wang Y, Shi J, Marques F C, Berry J J, Tumas W, Lany S, Stevanović V, Toney

M F and Buonassisi T 2017 Perovskite-Inspired Photovoltaic Materials: Toward Best Practices in Materials Characterization and Calculations *Chem. Mater.* **29** 1964-88
[362] Guillén E, Ramos F J, Anta J A and Ahmad S 2014 Elucidating Transport-Recombination Mechanisms in Perovskite Solar Cells by Small-Perturbation Techniques *J. Phys. Chem. C* **118** 22913-22
[363] Schelhas L T, Christians J A, Berry J J, Toney M F, Tassone C J, Luther J M and Stone K H 2016 Monitoring a Silent Phase Transition in $CH_3NH_3PbI_3$ Solar Cells via Operando X-ray Diffraction *ACS Energy Lett.* **1** 1007-12